Utility of SARS-CoV-2 infection models using *in vitro* and *in vivo* ACE2-lentivirus transduction

Daniel J. Rawle[1*], Thuy Le[1], Troy Dumenil[1], Kexin Yan[1], Bing Tang[1], Cameron Bishop[1], Andreas Suhrbier[1,2].

[1] Immunology Department, QIMR Berghofer Medical Research Institute, Brisbane, Queensland. 4029, Australia.
[2] Australian Infectious Disease Research Centre, GVN Center of Excellence, Brisbane, Queensland 4029 and 4072, Australia.

[*]Corresponding author. Email: Daniel.Rawle@qimrberghofer.edu.au

SUMMARY

SARS-CoV-2 uses the human ACE2 (hACE2) receptor, with mouse ACE2 (mACE2) unable to support infection. Herein we describe an ACE2-lentivirus system and illustrate its utility for *in vitro* and *in vivo* SARS-CoV-2 infection models. Transduction of non-permissive cell lines with hACE2 imparted replication competence, and transduction with mACE2 containing N30D, N31K, F83Y and H353K substitutions, to match hACE2, rescued SARS-CoV-2 replication. hACE2-lentivirus transduction of C57BL/6J, IFNAR$^{-/-}$ and IL-28RA$^{-/-}$ mice lungs illustrated that removing type I or III interferon responses had no significant effect on virus replication. However, RNA-Seq analyses illustrated they were required for the inflammatory responses, which were similar to those seen in COVID-19 patients. We also illustrate the utility of hACE2 transduction for vaccine evaluation in C57BL/6J mice. In summary, we establish a hACE2-lentivirus mouse model which has broad application in SARS-CoV-2 research, while also offering the inherent advantages of lentiviral transduction such as stable genomic integration.

KEYWORDS

SARS-CoV-2; COVID-19; lentivirus; ACE2; GM mice; vaccination; mutations; interferon; inflammation; RNA-seq

INTRODUCTION

Severe acute respiratory syndrome coronavirus 2 (SARS-CoV-2) has spread rapidly into a global pandemic (Wu et al., 2020a). SARS-CoV-2 infection can be asymptomatic, but is also the etiological agent of coronavirus disease 2019 (COVID-19), with acute respiratory distress syndrome (ARDS) representing a common severe disease manifestation (Guan et al., 2020). The SARS-CoV-2 pandemic has sparked unprecedented global research into understanding mechanisms of virus replication and disease pathogenesis, with the aim of generating new vaccines and treatments. Key to these efforts has been the development of animal models of SARS-CoV-2 infection and COVID-19 disease (Muñoz-Fontela et al., 2020).

The receptor binding domain (RBD) of the spike glycoprotein of SARS-CoV-2 binds human Angiotensin-Converting Enzyme 2 (hACE2) as the primary receptor for cell attachment and entry (Zhao et al., 2020). Mice do not support productive virus replication because the SARS-CoV-2 spike does not bind to mouse ACE2 (mACE2) (Zhou et al., 2020). Expression of hACE2 in mice via a transgene allows SARS-CoV-2 infection and provides mouse models that recapitulate aspects of COVID-19. In such models hACE2 is expressed under control of various promoters, including K18 (Golden et al., 2020; McCray et al., 2007; Moreau et al., 2020; Oladunni et al., 2020; Rathnasinghe et al., 2020; Winkler et al., 2020; Yinda et al., 2021), mACE2 (Bao et al., 2020; Sun et al., 2020b), HFH4 (Jiang et al., 2020b), or chicken β-actin (Tseng et al., 2007). These mouse models all differ in various aspects including level of virus replication, disease manifestations and tissue tropisms (Muñoz-Fontela et al., 2020), but do not provide a simple mechanism whereby genetically modified (GM) or knock-out mice can be exploited for SARS-CoV-2/COVID-19 research. Two systems that do allow the latter, involve transient hACE2 expression in mouse lungs using adenovirus vectors (Ad5) or adeno-associated virus (AAV), which impart the capacity for productive SARS-CoV-2 replication in mouse lungs (Hassan et al., 2020; Israelow et al., 2020; Rathnasinghe et al., 2020). A third model involves use of mouse adapted SARS-CoV-2 (Dinnon et al., 2020; Gu et al., 2020; Leist et al., 2020), although use of this mutated virus may complicate evaluation of interventions targeting human SARS-CoV-2.

Lentivirus-mediated gene expression in mice lung epithelium has been investigated as a treatment for cystic fibrosis and provides long term expression of the cystic fibrosis transmembrane conductance regulator (CFTR) (Alton et al., 2017b; Buckley et al., 2008; Copreni et al., 2010; Copreni et al., 2004; Kremer et al., 2007; Limberis et al., 2010; Wilson, 2004). These studies demonstrated that VSV-G pseudotyped lentivirus can transduce mouse airway epithelial cells and their progenitors resulting in long-term gene expression. Herein we describe an ACE2-lentiviral system that conveys SARS-CoV-2 replication competence *in vitro* and allows productive infection of mouse lungs *in vivo*. We illustrate that GM mice can thereby be accessed for SARS-CoV-2/COVID-19 research, with experiments using IFNAR$^{-/-}$ and IL-28RA$^{-/-}$ mice showing the importance of type I and III IFN responses for SARS-CoV-2-induced inflammation. We also illustrate the use of hACE2-lentiviral transduction of lungs of wild-type C57BL/6J mice for evaluation of vaccines.

RESULTS

hACE2-lentiviruses for evaluating the role of RBD binding residues

hACE2 coding sequence (optimized for mouse codon usage) was cloned into the dual promoter lentiviral vector pCDH-EF1α-MCS-BGH-PGK-GFP-T2A-Puro (herein referred to as pCDH) (Figure 1A), which had been modified to contain the full length EF1α promoter. Previous studies have shown that the EF1α promoter effectively drives gene expression after intranasal VSV-G pseudotyped lentivirus transduction of mouse lungs (Alton et al., 2017a). The GFP marker and puromycin resistance gene (cleaved from GFP by T2A) are expressed from a separate 3-phosphoglycerate kinase (PGK) promoter (Figure 1A). VSV-G pseudotyped pCDH-hACE2 lentivirus was produced by co-transfection of the lentiviral vector with VSV-G and Gag-Pol-Rev plasmids in HEK293T cells, and was used to transduce HEK293T (human embryonic

kidney) cells followed by puromycin selection. HEK293T cells do not express hACE2 (Crawford et al., 2020) and therefore do not support SARS-CoV-2 replication, whereas HEK293T cells transduced with hACE2 supported significant virus replication (Figure 1B). A T92Q mutation in hACE2 was introduced to determine if removing the N90 glycosylation motif increased SARS-CoV-2 replication, as computer-based modelling predicted enhanced affinity for spike RBD with removal of this glycan (Chan et al., 2020; Mehdipour and Hummer, 2020). We also introduced K31N/K353H and T27Y/L79Y/N330Y mutations into hACE2 as these changes were predicted by computer modeling to reduce and enhance affinity for spike RBD (Chan et al., 2020), respectively. HEK293T cells expressing these aforementioned hACE2 mutations did not significantly affect SARS-CoV-2 replication (Figure 1B), illustrating that *in silico* affinity predictions do not always translate to differences in virus replication.

Characterizing residues responsible for the inability of mACE2 to support SARS-CoV-2 replication

The ACE2-lentivirus system was used to introduce amino acid substitutions into mACE2 to identify the amino acids that are responsible for restricting SARS-CoV-2 replication in mACE2-expressing cells. Analysis of crystal structures and species susceptibilities has suggested residues that may be responsible for the differences in binding of the RBD to hACE2 and mACE2 (Alexander et al., 2020; Damas et al., 2020; Griffin et al., 2020; Rodrigues et al., 2020; Wang et al., 2020). Based on these *in silico* studies, we identified seven residues potentially responsible for the human-mouse differences. mACE2-lentivirus vectors were then generated that contained all seven substitutions (N30D/N31K/T79L/S82M/F83Y/A329E/H353K), with two further vectors constructed to identify the minimum requirements for SARS-CoV-2 replication. The latter contained a subset of the seven changes; four amino acid changes (N30D/N31K/F83Y/H353K) and two amino acid changes (N31K/H353K).

As expected HEK293T cells expressing mACE2 did not support productive SARS-CoV-2 replication, and CPE was not observed. In contrast, all three mACE2 mutants significantly rescued virus replication and infection resulted in CPE (Figure 1C-D). However, virus replication was significantly lower for cells expressing mACE2 with only two substitution (N31K/H353K) (Figure 1C) and infection produced less CPE (Figure 1D). Thus two amino acid changes (N31K and H353K) in mACE2 were sufficient to support SARS-CoV-2 replication; however, at least four changes (N30D/N31K/F83Y/H353K) were required for virus replication and CPE to be comparable to cells expressing hACE2.

Thus of all the potential interactions between the RBD and ACE2 previously identify by X ray crystallography and of all the amino acid differences between human and mouse ACE2 (Damas et al., 2020; Wang et al., 2020), it emerges 4 are key to determining infectivity differences for cells expressing hACE2 or mACE2. In the aforementioned crystal structures, hACE2-D30 interacts with S-K417 via a salt bridge, hACE2-K31 interacts with S-Q493, hACE2-Y83 interacts with S-N487, and hACE2-K353 forms hydrogen bonds with S-G496 and S-G502 (Figure 1E). Our studies highlight the utility of the ACE2-lentivirus system for studying the role of ACE2 residues in productive SARS-CoV-2 infections.

hACE2-lentivirus transduction of mouse cell lines imparts SARS-CoV-2 replication competence

To determine whether hACE2-lentivirus transduction could make mouse cell lines SARS-CoV-2 replication competent and thus available for SARS-CoV-2 research, 3T3 (mouse embryonic fibroblasts) and AE17 (mouse lung mesothelioma cell line) cells were transduced with hACE2. Significant virus replication was seen in transduced cells (Supplementary Figure 1), although somewhat lower than that seen in transduced HEK293T cells. Overt CPE was not seen (Supplementary Figure 1). This illustrates that the hACE2-lentivirus system can be used for mouse cell lines, but that the efficiency of viral replication may be cell line or cell type dependent.

SARS-CoV-2 replication in hACE2-lentivirus transduced C57BL/6J, IFNAR$^{-/-}$ and IL-28RA$^{-/-}$ mice lung

To illustrate the utility of the hACE2-lentivirus system for use in GM mice, we investigated the role of type I and type III IFN receptor signaling in SARS-CoV-2 infections. C57BL/6J, IFNAR$^{-/-}$ and IL-28RA$^{-/-}$ were inoculated intranasally (i.n.) with 1.2-2.2×10^4 transduction units of hACE2-lentivirus, equivalent to approximately 190-350 ng of p24 per mice (Figure 2A). An hour prior to administration of lentivirus, mice were treated i.n. with 1% lysophosphatidylcholine (LPC) to enhance transduction efficiency (Kremer et al., 2007; Limberis et al., 2002). One week later mice were challenged with SARS-CoV-2 (10^5 $CCID_{50}$ i.n. per mice), and lungs were collected at 2, 4 and 6 days post infection for C57BL/6J and IFNAR$^{-/-}$ mice and day 2 for IL-28RA$^{-/-}$ mice (Figure 2A). Mice did not display overt clinical symptoms or weight loss (Figure 2B), consistent with some studies using Ad5-hACE2 (Rathnasinghe et al., 2020), but not others (Sun et al., 2020a). RT-qPCR analyses indicated similar levels of hACE2 mRNA after transduction of mouse lungs in each of the 3 mouse strains, with expression maintained over the 6 day course of the experiment at levels significantly higher than untransduced mice (Figure 2C).

Lungs from infected C57BL/6J, IFNAR$^{-/-}$ and IL-28RA$^{-/-}$ were analyzed for infectious virus tissue titers. Untransduced lungs showed no detectable virus titers (Figure 2D), whereas hACE2-lentivirus transduced lungs showed significant viral titers ranging from 10^2 to 10^5 $CCID_{50}$/g for all strains of mice on day 2, with titers dropping thereafter (Figure 2D). Viral RNA levels were measured using RT-qPCR, with untransduced lungs showing low and progressively decaying levels post-inoculation (Figure 2E). For all hACE2-lentivirus transduced lungs, significantly elevated and persistent viral RNA levels were seen for all strains and at all time points by RT-qPCR (Figure 2E). Reducing viral titers and lingering viral RNA have been reported previously for K18-hACE2 mice (Winkler et al., 2020) and has also been suggested in human infections (Jefferson et al., 2020). RNA-Seq also illustrated that virus replication in hACE2-lentivirus transduced lungs, K18-hACE2 transgenic mice and Ad5-hACE2 transduced lungs (Sun et al., 2020a) were not significantly different when normalized to hACE2 mRNA expression (Figure 2F), suggesting comparable hACE2 translation efficiencies and SARS-CoV-2 replication efficiencies in these different expression systems.

Importantly, no significant differences in viral loads emerged between C57BL/6J, IFNAR$^{-/-}$ and IL-28RA$^{-/-}$ mice (Figure 2D, E). This remained true even when viral RNA levels were normalized to hACE2 mRNA levels (Supplementary Figure 2). Similar results were obtained by RNA-Seq, with viral read counts not significantly different for the 3 mouse strains (Supplementary Figure 3A-D). Thus using three different techniques, no significant effects on viral replication could be seen in mice with type I or type III IFN receptor deficiencies.

SARS-CoV-2 replication in hACE2-lentivirus transduced mice lung induces inflammatory signatures by day 2 post-infection

To determine the innate responses to SARS-CoV-2 replication in hACE2-transduced mouse lungs, gene expression in lungs of infected hACE2-transduced mice was compared with infected untransduced mice on day 2 post-infection using RNA-Seq. Differentially expressed genes (DEGs) between these groups were identified using a false discovery rate (FDR, or q value) threshold of <0.05 (Figure 3A; Supplementary Table 1A-C). Of the 110 DEGs, 95 were upregulated, with ≈40% of these classified as type I IFN-stimulated genes (ISGs) as classified by Interferome (using conservative settings that only included genes validated *in vivo* for mice) (Figure 3B, full list in Supplementary Table 1D). Type III ISGs are known to be poorly annotated in this database, and so this analysis likely under-estimates the number of such ISGs.

Ingenuity Pathway Analysis (IPA) of the 110 DEGs produced a series of pro-inflammatory Upstream Regulators (USRs) (Supplementary Table 1E-F) and included Th1, Th2 and Th17-associated

cytokine USRs, as well as type I IFN USRs (Figure 3C). SARS-CoV-2-specific T cells in humans were reported to be predominantly Th1-associated, but Th2-associated cytokines were also identified (Weiskopf et al., 2020). A cytokine and type I IFN DEG list has been published for a RNA-Seq analysis of SARS-CoV-2 infected K18-hACE2 transgenic mice (Winkler et al., 2020). These DEG lists were used to interrogate the full pre-ranked (fold change) gene list (Figure 3A, Supplementary Table 1B) by Gene Set Enrichment Analysis (GSEA). Significant enrichments were observed (Figure 3D), indicating similar cytokine and type I interferon (IFN) responses after SARS-CoV-2 infection of K18-hACE2 transgenic and hACE2-lentivirus transduced mice.

IPA *Diseases and Functions* analysis of the 110 DEGs revealed a series of annotations dominated by cellular infiltration and innate responses signatures (Figure 3E, Supplementary Table 1G-H). Several of the annotations were associated with monocytes and macrophages (Figure 3E), consistent with a previous report showing that inflammatory monocyte-macrophages were the major source of inflammatory cytokines in mouse adapted SARS-CoV infected mice (Channappanavar et al., 2016). The cellular infiltrates in COVID-19 patient lungs is also dominated by monocyte-macrophages with a suggested role in severe disease (Pence, 2020). Innate immune signaling was also the dominant signature in other analyses including GO Biological Processes and Cytoscape (Supplementary Table 1I-J).

GSEA analysis using the >31,000 gene signatures available from the molecular signatures database (MSigDB), indicated significant negative enrichment (negative NES scores) of gene sets associated with translation and mitochondrial electron transport chain function (Supplementary Table 1K). Translation inhibition by SARS-CoV-2 Nsp1 via the blocking of mRNA access to ribosomes has been reported previously (Banerjee et al., 2020; Schubert et al., 2020). SARS-CoV-2 down-regulation of genes associated with cellular respiration and mitochondrial function has also been shown in human lung (Miller et al., 2021).

DEGs from human COVID-19 lung (Blanco-Melo et al., 2020) were also enriched in our hACE2-lentivirus transduced mouse lungs, and analysis of the core enriched genes indicated the similarity was due to cytokine, IFN, chemokine and inflammatory signaling genes (Figure 3F, Supplementary Table 1L-M). Another human COVID-19 lung dataset was also interrogated (Wu et al., 2020b) and the results again illustrated enrichment of immune-related DEGs in the hACE2-lentivirus transduced mice (Supplementary Table 1N).

Overall these analyses illustrate that SARS-CoV-2 infection in hACE2-lentivirus transduced C57BL/6J mice lungs significantly recapitulate responses seen in other murine models and in COVID-19 patients.

Day 6 post-infection is characterized by inflammation resolution and tissue repair signatures

To determine how response profiles progress in the hACE2-lentivirus model, RNA-Seq was used to compare lungs on day 2 with lungs on day 6 post-infection, with day 6 broadly representing the time of severe lung disease in the K18-hACE2 model (Winkler et al., 2020). As noted above (Figure 2D), the virus titers had dropped in hACE2-lentivirus transduced mice lung over this time period by ≈2.8 logs, and severe disease (typically measured by weight loss) was not evident in this hACE2-lentivirus model (Figure 2B). In both hACE2-lentivirus transduced and untransduced C57BL/6J mice there was a clear evolution of responses from day 2 to day 6 post-infection; however, DEGs obtained from the former were largely distinct from DEGs obtained from the latter (Figure 4A). The RNA-Seq data thus illustrated that the DEGs associated with virus infection were distinct from those associated with virus inoculation (Figure 4A). RNA-Seq of infected lungs provided 551 DEGs, 401 up-regulated and 150 down-regulated (Figure 4B, Supplementary Table 2A-C).

IPA USR analyses of the 551 DEGs showed a clear reduction in inflammatory cytokine annotations, although the IL4 signature remained a dominant feature on day 6 (Figure 4C, Supplementary

Table 2D-E). A Th2 skew and IL-4 have both been associated with lung damage in COVID-19 patients (Vaz de Paula et al., 2020). On day 6 there was an up-regulation of USRs primarily associated with tissue repair (Figure 4D, Supplementary Table 2F); MAPK1 (also known as ERK) and MAPK9 (Lavoie et al., 2020), BMP7 (Sountoulidis et al., 2012), TCF7L2 (Zhu et al., 2015), and KLF4 (Lin et al., 2017; Raslan and Yoon, 2020). B and T cell-associated USRs were also seen (Figure 4D, green circles) (Duperray et al., 1990; Nechanitzky et al., 2013; Wang et al., 2010), consistent with development of an adaptive immune response. A relatively minor PARP1 signature was identified (Figure 4D), with PARP inhibitors being considered for COVID-19 therapy (Badawy, 2020; Curtin et al., 2020). A strong signature associated with estrogen receptor 1 (ESR1) was observed (Figure 4D), with estrogen having anti-inflammatory properties and believed to be associated with reduced COVID-19 severity in women (Jin et al., 2020; Peckham et al., 2020; Pinna, 2021), and reduced SARS-CoV disease severity in female mice (Channappanavar et al., 2016; Channappanavar et al., 2017). Follicle stimulating hormone (FSH) (Figure 4D) stimulates estrogen production, and inhibin subunit alpha (INHA) is involved in the negative feedback of FSH production (Nicks et al., 2010). IPA Diseases and Functions analysis, Cytoscape, and GO Biological Processes analyses further supported the contention that on day 6 inflammation had abated and tissue repair was underway (Supplementary Table 2G-L).

The >31,000 gene sets available in MSigDB were used to interrogate the complete gene list (pre-ranked by fold change) for day 6 versus day 2 (Supplementary Table 2B) by GSEA. A highly significant negative enrichment for inflammatory response, and a highly significant positive enrichment for cilium development was seen (Figure 4E). Cilia in mammals are found in the lining of the respiratory epithelium. These GSEAs thus provide further support for the conclusion above, together arguing that in the hACE2-lentivirus model, day 6 post infection is characterized by inflammation resolution and tissue repair.

Type I and III IFN signaling is required for SARS-CoV-2-induced lung inflammation

To determine what responses to SARS-CoV-2 infection are dependent on type I IFN signaling, the lentivirus system was used to analyze IFNAR$^{-/-}$ mice lung using RNA-Seq. IFNAR$^{-/-}$ and C57BL/6J mice were transduced with hACE2-lentivirus and were then infected with SARS-CoV-2 and lungs harvested for RNA-Seq on days 2 and 6 post-infection. The largest impact of type I IFN signaling deficiency was seen on day 2 post infection (Figure 5A), consistent with disease resolution on day 6 (Figure 4C-E). The total number of DEGs for IFNAR$^{-/-}$ versus C57BL/6J mouse lungs on day 2 was 192, with most of these down-regulated (Figure 5A, Supplementary Table 3A-C). Viral reads were not significantly different between these two mouse strains (Figure 5A), confirming that knocking out type I IFN signaling is insufficient to significantly affect SARS-CoV-2 replication (Frieman et al., 2010).

We showed in Figure 3 that RNA-Seq analysis revealed 110 DEGs associated with inflammatory responses when hACE2-transduced versus untransduced C57BL/6J mouse lungs on day 2 post infection were compared. When the same comparison was made for hACE2-lentivirus transduced versus untransduced lungs in SARS-CoV-2 infected IFNAR$^{-/-}$ mice, only 1 DEG (Kcnk5) was identified (Figure 5B). This clearly illustrated that the inflammatory responses on day 2 in C57BL/6J mice (Figure 3C) required intact type I IFN signaling.

As a control, the number of DEGs for IFNAR$^{-/-}$ mice versus C57BL/6J in untransduced lungs was determined. Although virus replication (hACE2-lentivirus transduced lung) provided 192 DEGs, virus inoculation (untransduced lung) provided only 16 DEGs (Figure 5C). Thus again, virus inoculation had a limited effect on these analyses, with DEGs largely associated with virus infection.

Type III IFN is thought to act as a first-line of defense against infection at epithelial barriers, with the more potent and inflammatory type I IFN response kept in reserved in the event the first line of defense is breached (Galani et al., 2017; Lazear et al., 2019). As type III IFN signaling has been

implicated in reducing SARS-CoV-2 infection *in vitro* (Vanderheiden et al., 2020), the aforementioned analyses on day 2 was repeated in IL-28RA$^{-/-}$ mice. Viral reads were not significantly different between these two mouse strains (Figure 5D), confirming that knocking out type III IFN signaling was insufficient to significantly affect SARS-CoV-2 replication (Boudewijns et al., 2020; Frieman et al., 2010). The DEG list for IL-28RA$^{-/-}$ versus C57BL/6J mice comprised 132 genes (Supplementary Table 4A-C), of which 84 were down-regulated (Figure 5D). Perhaps surprisingly, the DEGs were mostly different from that seen in IFNAR$^{-/-}$ mice (Figure 5D), arguing that the ISGs stimulated by type I and III IFNs are largely distinct.

The majority (90%) of the 178 down-regulated DEGs in IFNAR$^{-/-}$ versus C57BL/6J mice on day 2 post infection were ISGs as defined by Interferome (using *in vivo* and mouse only settings) (Figure 5E, top and Supplementary Table 3D). Of the 84 down-regulated genes in IL-28RA$^{-/-}$ lungs, only 27% were identified as ISGs (Figure 5E, bottom and Supplementary Table 4D). However, there are no annotations in the Interferome database for type III ISGs in mice, and changing the settings to include human data (which is also under-annotated for type III IFN) did not increase the number of type III ISGs in our search using down DEGs from IL-28RA$^{-/-}$ lungs.

To determine the pathways regulated by type I and III IFN in response to SARS-CoV-2 infection, IPA USR analyses was performed on DEG lists from day 2 for hACE2-lentivirus transduced lungs for IFNAR$^{-/-}$ versus C57BL/6J (192 DEGs) and IL-28RA$^{-/-}$ versus C57BL/6J (132 DEGs). IPA USR signatures associated with pro-inflammatory cytokine signaling were significantly reduced in both IFNAR$^{-/-}$ and, to a lesser extent, IL-28RA$^{-/-}$ mice when compared to C57BL/6J mice (Figure 5F, full lists in Supplementary Table 3E and 4E). The USR annotations for type I and III IFN receptor deficiencies were largely similar (Figure 5F), although they arose from a largely distinct set of DEGs (Figure 5D). This likely reflects expression of type I and type III IFN by different cell types with differing response profiles to the same cytokines (Lazear et al., 2019).

Taken together these results illustrate that while there was no significant effects on viral replication, lungs from type I and type III IFN receptor knockout mice both had a significantly blunted acute pro-inflammatory response following SARS-CoV-2 infection. The importance of type I IFN for inflammation was reported previously using the AAV-hACE2 system (Israelow et al., 2020).

Immunization with infectious or UV-inactivated SARS-CoV-2 protects against virus infection

To evaluate the utility of the hACE2-lentivirus mouse model of SARS-CoV-2 replication for vaccine studies, C57BL/6J mice were immunized twice subcutaneously (s.c.) with either infectious SARS-CoV-2 or UV-inactivated SARS-CoV-2 (Takasuka et al., 2004) formulated with adjuvant (Figure 6A). Serum SARS-CoV-2 neutralization titers were determined post-boost, and revealed all mice had significant serum neutralization titers (Figure 6B), comparable with the higher end levels seen in people with past SARS-CoV-2 infections (Wajnberg et al., 2020). On day 2 post challenge all mice were sacrificed. All mouse lungs had detectable hACE2 mRNA by RT-qPCR, with levels higher in unvaccinated mice (Figure 6C), likely due to immune cell infiltrates (see below) diluting hACE2 mRNA. Mice immunized with either infectious or UV-inactivated SARS-CoV-2 showed significant reductions in viral RNA levels by RT-qPCR (Figure 6D) in tissue titrations (Figure 6E) and by RNA-Seq read counts (Figure 6F). These immunizations thus protected mice against significant viral infections and demonstrated the utility of hACE2-lentivirus transduced mice as a model for vaccine evaluation.

Lungs harvested on day 2 were also analyzed by RNA-Seq (Supplementary Table 5A-B), with 1376 DEGs identified for infectious virus immunization versus unimmunized (DEGs in Supplementary Table 5C). The DEGs were analyzed by IPA canonical pathways, USR analysis, and the Diseases and Functions feature, which all showed infiltration signatures, dominated by T cell annotations (Supplementary Table 5D-F). This was confirmed by GSEA of human blood transcription modules (Li et al., 2014) against the pre-ranked (by fold change) gene list for immunized versus unvaccinated mice

(Supplementary Table 5G). This showed the expected enrichment of T cell and B annotations in immunized mice (Figure 6F), and illustrated that protection against virus replication in lungs of immunized mice was associated with a significant infiltration of lymphocytes. This aligns with studies that suggest COVID-19 patients that induce an early SARS-CoV-2-specific T cell response have rapid viral clearance and mild disease (Tan et al., 2021).

DISCUSSION

Herein we describe a hACE2-lentivirus transduction system that allows the use of C57BL/6J and GM mice for SARS-CoV-2/COVID-19 research. Virus titer in hACE2-lentivirus transduced mice lung were comparable to other studies using mice transduced with Ad5 or AAV expressing hACE2 (Hassan et al., 2020; Israelow et al., 2020; Rathnasinghe et al., 2020). These transduction methodologies avoid the fulminant brain infection seen in K18-hACE2 mice, with infection of this organ the major contributor to mortality in the K18-hACE2 model (Carossino et al., 2021; Kumari et al., 2020). The key advantage of lentiviral over adenoviral systems is the integration of the lentiviral payload into the host cell genome, thereby providing long-term stable expression. The hACE2-lentivirus thus provides a new option for studying SARS-CoV-2 infection that can be readily applied using standard lentivirus technology. We characterize the lentivirus-hACE2 model of SARS-CoV-2 infection in C57BL/6J mice, and illustrate the use of lentivirus-hACE2 to assess the role of type I and type III IFNs in virus control and inflammatory responses using IFNAR$^{-/-}$ and IL-28RA$^{-/-}$ mice, respectively. We also illustrate the use of C57BL/6J mice transduced with lentivirus-hACE2 for SARS-CoV-2 vaccine evaluation.

The lentivirus-hACE2 C57BL/6J mouse model of SARS-CoV-2 infection shares many cytokine signatures with those seen in human COVID-19 patients; IL-2, IL-10, IL-6, TNFα, IL-4, IL-1β, IFNγ and CSF3 signatures were found in SARS-CoV2-infected lentivirus-hACE2 transduced C57BL/6J mice on day 2 post infection, and elevated levels of these cytokines are found in COVID-19 patients (Han et al., 2020; Huang et al., 2020). Several of these cytokines have been implicated as mediators of COVID-19; for instance, IL-6 (Herold et al., 2020; Masiá et al., 2020; Xia et al., 2020), IL-4 (Vaz de Paula et al., 2020), IL-10 (Lu et al., 2021) and IFNγ (Gadotti et al., 2020). On day 6 post infection the lentivirus-hACE2 C57BL/6J mouse model showed a series of signatures associated with tissue repair. Thus our RNA-Seq analyses illustrated that this model involves an acute inflammatory disease followed by resolution and tissue repair.

hACE2-lentivirus transduction in IFNAR$^{-/-}$ and IL-28RA$^{-/-}$ mice was used to confirm that type I IFN signaling (Israelow et al., 2020) and show that type III IFN signaling are involved in driving inflammatory responses. Virus replication was not significantly affected in IFNAR$^{-/-}$ and IL-28RA$^{-/-}$ mice, largely consistent with other studies using different model systems, which indicate that knocking out both pathways (STAT1$^{-/-}$, STAT2$^{-/-}$, or combined IFNAR$^{-/-}$/IL-28RA$^{-/-}$) is required before an impact on virus replication is seen (Boudewijns et al., 2020; Frieman et al., 2010; Israelow et al., 2020; Mahlakõiv et al., 2012). A high level of cross-compensation is thus implicated, as is described in influenza infection (Galani et al., 2017). *In vitro* experiments show that SARS-CoV-2 replication is sensitive to type I and III IFNs, although infection does not stimulate particularly high levels of IFN (Felgenhauer et al., 2020; Nguyen et al., 2021; Vanderheiden et al., 2020). A number of SARS-CoV-2 encoded proteins inhibit IFN production and signaling (Jiang et al., 2020a; Miorin et al., 2020; Xia et al., 2020). In infected cells, such inhibition of signaling would limit the antiviral activity of IFNs, as well as limiting the positive feedback amplification that is needed for high level IFN production (Hall and Rosen, 2010). IFN therapies have been proposed for COVID-19 patients (Monk et al., 2020) and such treatment may induce an antiviral state in uninfected cells, thereby perhaps limiting viral spread if given prophylactically or early during the course of infection (Park and Iwasaki, 2020). However, caution might be warranted for such therapy

during later stage COVID-19 as type I and III IFN signaling are shown herein to drive inflammatory responses during SARS-CoV-2 infection, and are also known to have pro-inflammatory activities in other settings (Hall and Rosen, 2010).

Herein we also illustrate the use of the hACE2-lentivirus system to study the role of ACE2 residues on SARS-CoV-2 replication *in vitro*. Only four "mouse-to-human" changes in mACE2 (N30D, F83Y, N31K, H353K) enabled full SARS-CoV-2 replication to levels similar to those seen for infection of hACE2-expressing cells. These results suggest a CRISPR mouse with these substitutions would be able to support SARS-CoV-2 infection and provide a model of COVID-19. Remarkably, a minimum of only two substitutions in mACE2 (N31K, H353K) were sufficient for partial restoration of SARS-CoV-2 infection. Changing the same resides in hACE2 to their mouse equivalents (K31N, K353H) did not affect virus replication compared to WT hACE2. Thus N31K and H353K allows binding of SARS-CoV2 to mACE2, but K31N and K353H does not impair binding to hACE2. Both K31N and K353H substitutions were shown to be deleterious for SARS-CoV2 binding by *in silico* analyses. However, the same analyses implicated >25 other residues in hACE2 binding (Chan et al., 2020), with many of these potentially able to compensate for the loss of native residues at K31 and K353.

In conclusion, we describe the development of a mouse model using intranasal hACE2-lentivirus transduction to sensitize mice lung to SARS-CoV-2 infection, which recapitulated cytokine signatures seen in other mouse models and COVID-19. We demonstrate broad applicability of this new mouse model in vaccine evaluation, GM mice infection, and *in vitro* evaluation of ACE2 mutants.

ACKNOWLEDGEMENTS

We thank Dr I Anraku for his assistance in managing the PC3 (BSL3) facility at QIMR Berghofer MRI. We thank Dr Alyssa Pyke and Mr Fredrick Moore (Queensland Health, Brisbane) for providing the SARS-CoV-2 isolate. We thank Dr. David Harrich for providing the lentivirus vector system. We thank Dr. Simon Phipps for providing the IL-28RA$^{-/-}$ mice. We thank Monash Genome Modification Platform for providing the plasmid containing the mouse-codon optimized human ACE2 gene. We thank Clive Berghofer and Lyn Brazil (and many others) for their generous philanthropic donations to support SARS-CoV-2 research at QIMR Berghofer MRI. A.S. holds an Investigator grant from the National Health and Medical Research Council (NHMRC) of Australia (APP1173880).

AUTHOR CONTRIBUTIONS

Conceptualization, D.J.R.; Methodology, D.J.R. and A.S.; Formal analysis, D.J.R., A.S., and T.D.; Investigation, D.J.R., T.L., K.Y., B.T.; Data curation, D.J.R., A.S., and T.D.; Writing – original draft, D.J.R.; Writing – review and editing, A.S. and D.J.R.; Visualization, D.J.R., A.S., T.D., and C.B; Supervision, D.J.R. and A.S., Project administration, D.J.R. and A.S.; Funding acquisition, A.S. and D.J.R.

DECLARATION OF INTERESTS

The authors declare no competing interests.

DATA AVAILABILITY

All raw sequencing data (fastq files) are available from the Sequence Read Archive (SRA), BioProject accession: PRJNA701678. All other data is available within the paper and supporting information files.

FIGURE LEGENDS

Figure 1. Mutational analyses of human and mouse ACE2 using ACE2-lentiviruses *in vitro*. A) Schematic of pCDH-EF1α-ACE2-BGH-PGK-GFP-T2A-Puro lentiviral vector. **B-C)** Growth kinetics of

SARS-CoV-2 over a three day time course in HEK293T cells transduced with WT or mutant hACE2 **(B)** or mACE2 **(C)** infected at MOI=0.1. Data is the mean of 1 (hACE2-T27Y/L79Y/N330Y and mACE2-N31K/H353K) or 2 (all others) independent experiments with 2-3 replicates in each and error bars represent SEM. Statistics was determined using Repeated Measures Two-Way ANOVA comparing untransduced (for B) or WT mACE2 (for C) with all others, and comparing mACE2-N30D/N31K/F83Y/H353K with mACE2-N31K/H353K. **D)** Inverted light microscopy images of HEK293T cells transduced with the indicated ACE2 lentivirus and infected with SARS-CoV-2 at MOI=0.1. Images were taken at day 3 post infection and were representative of triplicate wells. **E)** Crystal structure of the Spike RBD:hACE2 complex (PBD: 6M0J) viewed in PyMOL and highlighting key interactions (blue) between hACE2 (red) and Spike RBD (green).

Figure 2. SARS-CoV-2 replication in hACE2-lentivirus transduced C57BL/6J, IFNAR$^{-/-}$ and IL-28RA$^{-/-}$ mice lung. A) Timeline of lentivirus transduction of mice lung and SARS-CoV-2 infection. **B)** Percent weight loss for mice in C-E. Data represents the mean percent weight loss from day 0 and error bars represent SEM. **C)** RT-qPCR of mice lung RNA using primers for hACE2 (introduced by lentivirus transduction) normalized to mRPL13a levels. Data is for individual mice and is expressed as RNA copy number calculated against a standard curve for each gene. Horizontal line indicates cut-off for reliable detection, with all untransduced mice falling below this line. Statistics are by Kolmogorov Smirnov test compared to untransduced samples. **D)** Titer of SARS-CoV-2 in mice lung determined using $CCID_{50}$ assay of lung homogenate. Horizontal line indicates the limit of detection of 1.57 $\log_{10}$ $CCID_{50}$/g. Statistics are by Kolmogorov Smirnov test compared to untransduced mice. IFNAR$^{-/-}$ versus untransduced mice at day 2 post infection reaches significance by Kruskal-Wallis test (p=0.018). **E)** RT-qPCR of mice lung RNA using primers for SARS-CoV-2 E gene normalized to mRPL13a levels. Data is individual mice and is expressed as RNA copy number calculated using a standard curve. Statistics are by Kolmogorov Smirnov test compared to untransduced mice. C57BL/6J hACE2-transduced versus untransduced mice at day 4 post infection reaches significance by Kruskal-Wallis test (p=0.046). See Supplementary Figure 2 for SARS-CoV-2 RNA copies normalised to hACE2 copies. **F)** SARS-CoV-2 read counts (also see Supplementary Figure 3) normalized to hACE2 read counts from RNA-seq data for lentivirus-hACE2 transduced mice at day 2, K18-hACE2 transgenic mice at day 4, and Ad5-hACE2 transduced mice at day 2 (Sun et al., 2020a). Not significant by Kolmogorov Smirnov or Kruskal-Wallis tests.

Figure 3. SARS-CoV-2 replication in hACE2-lentivirus transduced mice lung induces inflammatory signatures by day 2 post-infection. A) Volcano plot of gene expression from RNA-seq analyses of lung at day 2 comparing mice with and without hACE2-lentivirus transduction. Genes were considered DEGs if they had a FDR value < 0.05 (above horizontal dotted line) (see Supplementary Table 1B-C for full gene and DEG lists). **B)** Interferome analysis of 95 up DEGs from 'A'. 38 of 95 up DEGs (40%) were ISGs. Red = type I IFN, blue = type II IFN, green = type III IFN (see Supplementary Table 1D for full Interferome ISG list). **C)** Cytokine signatures identified by IPA USR analysis (see Supplementary Table 1E-F for full and cytokine only USR lists) of 110 DEGs identified in 'A'. Circle area reflects the number of DEGs associated with each USR annotation. USRs were grouped into three categories; red = Th1 associated, green = Th2 associated, blue = Th17 associated, and black = pleiotropic/other. The vertical dotted line indicates activation z-score of 0. **D)** GSEAs for cytokine-related DEGs or type I IFN-related DEGs from Winkler et al. supplemental data (Winkler et al., 2020) against the pre-ranked all gene list (Supplementary Table 1B). Normalised enrichment score (NES) and nominal p-value are shown. **E)** IPA diseases and functions analysis (see Supplementary Table 1G-H for full lists) of 110 DEGs identified in 'A'. The 23 annotations with the most significant p-value and with an

activation z-score of >2 were plotted with dots/lines indicating activation z-score and bars indicating – $\log_{10}$ p-value. Annotations were grouped into two categories; cellular infiltration (blue) and innate responses (red). **F)** GSEA for DEGs from human COVID-19 lung versus healthy control from Blanco-Melo et al. (Blanco-Melo et al., 2020) against the pre-ranked (by fold change) all gene list (Supplementary Table 1B). Normalised enrichment score (NES) and nominal p-value are shown. Core enriched genes (see Supplementary Table 1L for full core enriched gene list) determined by GSEA were entered into Enrichr and the top 10 GO Biological Processes annotations sorted by p-value are shown (see Supplementary Table 1M for full GO processes list).

Figure 4. Day 6 post-infection is characterized by inflammation resolution and tissue repair signatures. A) Venn diagram for DEGs comparing day 6 versus 2 post infection with (red) and without (green) hACE2-lentivirus transduction. Number of DEGs that are FDR<0.05 are shown. Mean virus titer ($\log_{10}$ $CCID_{50}$/g) in lung tissue ± SEM (represents data shown in Figure 2D) is shown for hACE2 transduced mice at day 2 or 6 post infection. **B)** Volcano plot of gene expression from RNA-seq analyses of hACE2-lentivirus transduced lung RNA comparing day 6 with day 2 (see Supplementary Table 2B-C for gene and DEG lists). Genes were considered DEGs if they had a FDR value < 0.05 (above horizontal dotted line). **C)** Cytokine signatures identified by IPA USR analysis (see Supplementary Table 2D-E for full and cytokine only lists) of 551 DEGs identified in 'B' (Supplementary Table 2C). Circle area reflects the number of DEGs associated with each USR annotation. USRs were grouped into four categories; red = Th1 associated, green = Th2 associated, blue = Th17 associated, and black = pleiotropic/other. The vertical dotted line indicates activation z-score of 0. **D)** Upregulated USR signatures identified using IPA analysis (see Supplementary Table 2F) of 551 DEGs identified in 'B'. Circle area reflects the number of DEGs associated with each USR annotation. USRs (excluding chemicals) with an activation z-score of >2 are shown and were grouped into five categories; green = B cell function, blue = tissue repair – endocrine signaling, orange = tissue repair – growth factor, red = tissue repair – kinase, purple = tissue repair – Wnt signaling. **E)** Selected plots from GSEA of entire MSigDB database using pre-ranked (by fold change) 'all' gene list (Supplementary Table 2B). NES score and p-value is shown for the "GO_inflammatory_response" and "Wp_Genes_Related_To_Primary_Cilium_Development_Based_On_Crispr" annotations.

Figure 5. Type I and III IFN signaling is required for SARS-CoV-2-induced lung inflammation. A) Venn diagram for number of DEGs (FDR<0.05) between $IFNAR^{-/-}$ versus C57BL/6J mice at day 2 or day 6 (green). Mean $\log_{10}$ SARS-CoV-2 read count in RNA-seq data ± SEM is shown (red text = day 2, green text = day 6). **B)** Venn diagram for number of DEGs (FDR<0.05) between plus versus minus hACE2-lentivirus transduction comparing C57BL/6J (red) and $IFNAR^{-/-}$ (green) mice at day 2. **C)** Venn diagram for $IFNAR^{-/-}$ versus C57BL/6J mice at day 2 comparing hACE2-lentivirus transduced (red) or untransduced (green) mice. **D)** Venn diagram comparing $IFNAR^{-/-}$ versus C57BL/6J (red) and IL-$28RA^{-/-}$ versus C57BL/6J (blue) (see Supplementary Table 3B-C and 4B-C for full gene and DEG lists) mice at day 2 (all mice had received hACE2-lentivirus transduction). Mean $\log_{10}$ SARS-CoV-2 read count in RNA-seq data ± SEM is shown (red text = $IFNAR^{-/-}$, black text = C57BL/6J, blue text = IL-$28RA^{-/-}$). **E)** Interferome analysis of down DEGs from 'D'. See supplementary Table 3D and 4D for full Interferome ISG list. **F)** Signatures identified using IPA USR analysis of DEGs identified in 'D' for $IFNAR^{-/-}$ versus C57BL/6J (red) and IL-$28RA^{-/-}$ versus C57BL/6J (blue). Circle area reflects the number of DEGs associated with each USR annotation. Signatures were selected focusing on data previously identified in 'Figure 3C' (entire list is in Supplementary Table 3E and 4E).

Figure 6. Immunization with infectious or UV-inactivated SARS-CoV-2 protects against virus

infection. A) Timeline of mice immunization, lentivirus transduction and SARS-CoV-2 infection. **B)** Reciprocal 50% neutralization titers of naïve mice and infectious or UV SARS-CoV-2 immunized mice. Horizontal dotted line represents the limit of detection (1 in 10). Statistics are by Kolmogorov Smirnov test. **C)** RT-qPCR of mice lung RNA using primers for hACE2 introduced by lentivirus transduction normalized to mRPL13a levels. Data is individual mice and is expressed as RNA copy number calculated against a standard curve for each gene. Horizontal line indicates cut-off for reliable detection, with all hACE2-negative mice falling below this line. Statistics are by Kolmogorov Smirnov test. **D)** RT-qPCR of mice lung RNA using primers for SARS-CoV-2 E gene normalized to mRPL13a levels. Data is individual mice and is expressed as RNA copy number calculated against a standard curve for each gene. Statistics are by Kolmogorov Smirnov test. Unvaccinated versus UV-inactive CoV-2 vaccinated reaches significance by Kruskal-Wallis test (p=0.034). **E)** Titer of SARS-CoV-2 in mice lung determined using $CCID_{50}$ assay of lung homogenate. Horizontal line indicates the limit of detection of 1.57 $\log_{10}$ $CCID_{50}$/g. Statistics are by Kolmogorov Smirnov test. Unvaccinated versus UV-inactive CoV-2 vaccinated reaches significance by Kruskal-Wallis test (p=0.028). **F)** Mean $\log_{10}$ SARS-CoV-2 read count at day 2 post-infection in RNA-seq data ± SEM is shown (blue text = unvaccinated mice, red text = infectious SARS-CoV-2 immunized mice). GSEA for Blood Transcription Modules (BTMs) from Li et al. (Li et al., 2014) against the pre-ranked all gene list comparing unvaccinated versus infectious SARS-CoV-2 immunized (s.c) mice lung at day 2 (all mice had hACE2-lentivirus transduction). Selected BTM modules with a positive NES score and $p < 0.05$ are shown (full list in Supplementary Table 5). See Supplementary Table 5 for full gene and DEG lists and full downstream analyses lists.

STAR METHODS

Ethics statement

All mouse work was conducted in accordance with the "Australian code for the care and use of animals for scientific purposes" as defined by the National Health and Medical Research Council of Australia. Mouse work was approved by the QIMR Berghofer Medical Research Institute animal ethics committee (P3600, A2003-607). Mice were euthanized using CO_2 or cervical dislocation.

Cell lines and SARS-CoV-2 culture

Vero E6 (C1008, ECACC, Wiltshire, England; Sigma Aldridge, St. Louis, MO, USA), HEK293T (a gift from Michel Rist, QIMR Berghofer), Lenti-X 293T (Takara Bio), AE17 (a gift from Delia Nelson, Faculty of Health Sciences, Curtin Medical School), and NIH-3T3 (American Type Culture Collection, ATCC, CRL-1658) cells were cultured in medium comprising DMEM for Lenti-X 293T cells or RPMI1640 for all others (Gibco) supplemented with 10% fetal calf serum (FCS), penicillin (100 IU/ml)/streptomycin (100 μg/ml) (Gibco/Life Technologies) and L-glutamine (2 mM) (Life Technologies). Cells were cultured at 37°C and 5% CO_2. Cells were routinely checked for mycoplasma (MycoAlert Mycoplasma Detection Kit MycoAlert, Lonza) and FCS was assayed for endotoxin contamination before purchase (Johnson et al., 2005). The SARS-CoV-2 isolate was kindly provided by Queensland Health Forensic & Scientific Services, Queensland Department of Health, Brisbane, Australia. The virus (hCoV-19/Australia/QLD02/2020) was isolated from a patient and sequence deposited at GISAID (https://www.gisaid.org/; after registration and login, sequence can be downloaded from https://www.epicov.org/epi3/frontend#1707af). Virus stock was generated by infection of Vero E6 cells at multiplicity of infection (MOI)≈0.01, with supernatant collected after 2-3 days, cell debris removed by centrifugation at 3000 x g for 15 min at 4°C, and virus aliquoted and stored at -80°C. Virus titers were determined using standard $CCID_{50}$ assays (see below). The virus was determined to be mycoplasma free using co-culture with a non-permissive cell line (i.e. HeLa) and Hoechst staining as described (La Linn et al., 1995).

$CCID_{50}$ assays

Vero E6 cells were plated into 96 well flat bottom plates at $2x10^4$ cells per well in 100 µl of medium. For tissue titer, tissue was homogenized in tubes each containing 4 ceramic beads twice at 6000 x g for 15 seconds, followed by centrifugation twice at 21000 x g for 5 min before 5 fold serial dilutions in 100 µl RPMI1640 supplemented with 2% FCS. For cell culture supernatant, 10 fold serial dilutions were performed in 100 µl RPMI1640 supplemented with 2% FCS. 100 µl of serially diluted samples were added to Vero E6 cells and the plates cultured for 5 days at 37°C and 5% CO_2. The virus titer was determined by the method of Spearman and Karber (a convenient Excel $CCID_{50}$ calculator is available at https://www.klinikum.uni-heidelberg.de/zentrum-fuer-infektiologie/molecular-virology/welcome/downloads).

Lentivirus cloning

ACE2 genes were cloned into pCDH-EF1α-MCS-BGH-PGK-GFP-T2A-Puro Cloning and Expression Lentivector (System Biosciences, catalogue number CD550A-1), where the EF1α promoter was replaced with the full length EF1α using NheI and ClaI restriction enzymes (New England Biolabs). Human ACE2 coding sequence (codon optimized for mouse) was cloned into the pCDH lentivector with PCR fragments amplified using Q5® High-Fidelity 2X Master Mix (New England Biolabs) and the following primers; vector backbone (pCDH amplified with Forward 5'- TAAATCGGATCCGCGG -3' and Reverse 5'- AATTCGAATTCGCTAGC) and hACE2 insert (Forward 5'- GCTAGCGAATTCGAATTATGAGCAGCAGCTCTTGGC -3' and Reverse 5'- CCGCGGATCGCATTTATCAGAAGCTTGTCTGCACGT -3'). The pCDH fragment was digested with DpnI (New England Biolabs) and was purified using QIAquick Gel Extraction Kit (QIAGEN), as was the hACE2 fragment. Fragments were recombined using NEBuilder HiFi DNA Assembly Cloning Kit as per manufacturer instructions. This was transformed into NEB® 10-beta Competent E. coli (High Efficiency) (New England Biolabs) as per manufacturer instructions and plated on ampicillin agar plates overnight. Colony PCR was performed using Q5 High-Fidelity 2X Master Mix (New England Biolabs) and the hACE2 insert primers to identify a positive colony, which was grown in LB broth with ampicillin and plasmid was purified using NucleoBond Xtra Midi kit (Machery Nagel).

All ACE2 mutant coding sequences were ordered from Twist Bioscience/Decode Science containing EcoRI upstream and BamHI downstream. Fragments were amplified using the using Q5® High-Fidelity 2X Master Mix (New England Biolabs) and the following primers; Forward 5'- CCTGACCTTAGCGAATTCATG -3' and Reverse 5'- ACCTAGCCTCGCGGATC -3'. PCR fragments were purified using Monarch DNA Gel Extraction Kit (New England Biolabs), and were digested with EcoRI and BamHI (New England Biolabs), as was the pCDH vector before purification again with Monarch® DNA Gel Extraction Kit (New England Biolabs). The ACE2 fragment was ligated with pCDH vector using T4 DNA Ligase (New England Biolabs) as per manufacturer instructions and then transformed into NEB® 10-beta Competent E. coli (High Efficiency) (New England Biolabs) as per manufacturer instructions and plated on ampicillin agar plates overnight. Colonies were grown in LB broth with ampicillin and plasmid was purified using NucleoBond Xtra Midi kit (Machery Nagel). Plasmids were confirmed by PCR with the cloning primers above and fragments were gel purified and confirmed by Sanger sequencing with the forward primer.

Lentivirus production, titration and cell line transduction

ACE2 lentivirus was produced by co-transfection of HEK293T or Lenti-X HEK293T cells with the pCDH-ACE2 plasmid, VSV-G and Gag-Pol using Lipofectamine 2000 Reagent (Thermo Fisher Scientific) or Xfect Transfection Reagent (Takara Bio) as per manufacturer instructions. Supernatant was

collected 2 days after transfection and centrifuged at 500 x g for 10 min, and this was concentrated using Amicon Ultra-15 Centrifugal Filter Units with 100 kDa cutoff (Merck Millipore) as per manufacturer instructions. Lentivirus was titrated by serial dilution of lentivirus and incubating with 5000 HEK293T cells in 96 well plates with 8 µg/ml polybrene for 3 days followed by GFP detection by flow cytometry (BD Biosciences LSRFortessa). Transduction units (TU) per ml was calculated by percentage of 5000 cells that are GFP positive multiplied by the dilution. For example if 2 µl lentivirus gives 5% GFP positive cells, the TU/ml is ((5/100)*5000) * (1000/2) = 125,000 TU/ml. The p24 equivalent (ng/ml) was measured using Lenti-X GoStix Plus (Takara Bio) as per manufacturer instructions.
Cell lines were transduced by incubating with lentivirus and 8 µg/ml polybrene for 2-3 days followed by 5 µg/ml puromycin treatment until most resistant cells expressed GFP. Cells were then infected with SARS-CoV-2 at MOI 0.1 for 1 hr at 37°C, cells were washed with PBS and media replaced. Culture supernatant was harvested at the indicated timepoints and titered by $CCID_{50}$ assay as described.

UV-inactivated SARS-CoV-2 vaccine preparation and mice immunization

120 ml of SARS-CoV-2 was inactivated with at least 7650 J/m^2 UVC in a UVC 500 Ultraviolet Crosslinker (Hoefer). Virus was determined to be inactivated by incubation with Vero E6 cells for 4 days without development of CPE. UV-inactive SARS-CoV-2 was then partially-purified using a 20% sucrose cushion centrifuged at 175,000 x g for 3-4 hr using SW32Ti rotor (Beckman Coulter). The sample that has passed through the sucrose was collected and concentrated using Amicon Ultra-15 Centrifugal Filter Units with 100 kDa cutoff (Merck Millipore). For infectious SARS-CoV-2 immunization, virus was also concentrated using Amicon Ultra-15 Centrifugal Filter Units with 100 kDa cutoff (Merck Millipore). Mice were injected s.c. in the base of the tail with 100 µl of UV-inactive or infectious SARS-CoV-2 with 25 µg adjuvant in 50 µl made with the same ingredients as AS01 (Chlibek et al., 2013) as described previously (Yan et al., 2020). A boost was given 5-6 weeks after prime, and mice were bled to measure serum neutralizing titers 4-9 weeks after boost.

Neutralization assay

Mouse serum was heat inactivated at 56°C for 30 min and incubated with 100 $CCID_{50}$ SARS-CoV-2 for 2 hr at 37°C before adding 10^5 Vero cells/well in a 96 well plate to 200 µl. After 4 days cells were fixed and stained by adding 50 µl formaldehyde (15% w/v) and crystal violet (0.1% w/v) (Sigma-Aldrich) overnight. The plates were washed in tap water, dried overnight and 100 µl/well of 100% methanol added to dissolve the crystal violet and the OD was read at 595 nm using a 96-well plate reader (Biotek Synergy H4). The 50% neutralizing titers were interpolated from optical density (OD) versus dilution plots.

Mice intranasal lentivirus transduction and SARS-CoV-2 infection

C57BL/6J, $IFNAR^{-/-}$ (Swann et al., 2007) (originally provided by P. Hertzog, Monash University, Melbourne, VIC, Australia) and $IL\text{-}28RA^{-/-}$ (Ank et al., 2008; Galani et al., 2017) mice were bred in-house at QIMRB. Female mice were 8 weeks to 1 year old (age matched between groups) at the start of the experiment. Mice were anesthetized using isoflurane and 4 µl of 1% L-α-Lysophosphatidylcholine from egg yolk (Sigma Aldrich) in water was administered intranasally. After 1 hour mice were inoculated intranasally with approximately 2×10^4 TU of hACE2-pCDH lentivirus in 50 µl, and 1 week later challenged with 10^5 $CCID_{50}$ SARS-CoV-2 intranasally in 50 µl. Mice were sacrificed by cervical dislocation at day 2, 4 or 6 and lungs were collected. Right lung was immediately homogenized in tubes each containing 4 beads twice at 6000 x g for 15 seconds, and used in tissue titration as described above. Left lung was placed in RNAprotect Tissue Reagent (QIAGEN) at 4°C overnight then -80°C.
K18-hACE2 mice (McCray et al., 2007) were purchased from The Jackson Laboratory and bred in-house at QIMRB with C57BL/6J mice. Mice were genotyped using Extract-N-Amp Tissue PCR Kit (Sigma

Aldrich) according to manufacturer instructions with the following primers; Forward 5'-CTTGGTGATATGTGGGGTAGA-3' and Reverse 5'-CGCTTCATCTCCCACCACTT-3'. hACE2 positive mice were infected with 5×10^4 SARS-CoV-2 i.n. as above and lung RNA was harvested at day 4 for RNA-seq.

RT-qPCR

Mice lung was transferred from RNAlater to TRIzol (Life Technologies) and was homogenized twice at 6000 x g for 15 sec. Homogenates were centrifuged at 14,000 × g for 10 min and RNA was isolated as per manufacturer's instructions. cDNA was synthesized using ProtoScript II First Strand cDNA Synthesis Kit (New England Biolabs) and qPCR performed using iTaq Universal SYBR Green Supermix (Bio-Rad) as per manufacturer instructions with the following primers; SARS-CoV-2 E Forward 5'-ACAGGTACGTTAATAGTTAATAGCGT -3' and Reverse 5'- ATATTGCAGCAGTACGCACACA, hACE2 Forward 5'- GATCACGATTCCCAGGACG -3' and Reverse 5'- TCCGGCTGAACGACAACTC -3', mRPL13a (Schroder et al., 2010) Forward 5'- GAGGTCGGGTGGAAGTACCA -3' and Reverse 3'-TGCATCTTGGCCTTTTCCTT -3'. PCR fragments of SARS-CoV-2 E, ACE2 and mRPL13a using the same primers as above were gel purified and 10-fold serial dilutions of estimated copy numbers were used as standards in qPCR to calculate copies in samples reactions. SARS-CoV-2 E and ACE2 copies were normalized by mRPL13a copy number in each reaction. qPCR reactions were performed in duplicate and averaged to determine the copy number in each sample.

RNA-seq

TRIzol extracted lung RNA was treated with DNase (RNase-Free DNAse Set (Qiagen)) followed by purification using RNeasy MinElute Cleanup Kit (QIAGEN) as per manufacturer instructions. RNA concentration and quality was measured using TapeStation D1K TapeScreen assay (Agilent). cDNA libraries were prepared using the Illumina TruSeq Stranded mRNA library prep kit and the sequencing performed on the Illumina Nextseq 550 platform generating 75bp paired end reads. Per base sequence quality for >90% bases was above Q30 for all samples. The quality of raw sequencing reads was assessed using FastQC (Simons, 2010) (v0.11.8) and trimmed using Cutadapt (Martin, 2011) (v2.3) to remove adapter sequences and low-quality bases. Trimmed reads were aligned using STAR (Dobin et al., 2013) (v2.7.1a) to a combined reference that included the mouse GRCm38 primary assembly and the GENCODE M23 gene model (Harrow et al., 2012), SARS-CoV-2 isolate Wuhan-Hu-1 (NC_045512.2; 29903 bp) and the human ACE2 mouse codon optimized sequence (2418 bp). Mouse gene expression was estimated using RSEM (Li and Dewey, 2011) (v1.3.0). Reads aligned to SARS-CoV-2 and hACE2 were counted using SAMtools (Li et al., 2009) (v1.9). Differential gene expression in the mouse was analyzed using EdgeR (3.22.3) and modelled using the likelihood ratio test, glmLRT().

Analyses of K18-hACE2 and Ad5-hACE2 RNA-seq data

RNA-seq datasets generated from the Winkler et al. study (Winkler et al., 2020), and Sun et al. study (Sun et al., 2020a) were obtained from the Gene Expression Omnibus (GSE154104 and GSE150847 respectively) and trimmed using Cutadapt (v2.3). Trimmed reads were aligned using STAR (v2.7.1a) to a combined reference that included the mouse GRCm38 primary assembly and the GENCODE M23 gene model, SARS-CoV-2 isolate Wuhan-Hu-1 (NC_045512.2; 29903 bp) and the human ACE2 transcript variant 1 (NM_001371415.1; 3339 bp). Mouse gene expression was estimated using RSEM (v1.3.0). Reads aligned to SARS-CoV-2 and hACE2 were counted using SAMtools (v1.9). Differential gene expression in the mouse was analyzed using EdgeR (3.22.3) and modelled using the likelihood ratio test, glmLRT().

Pathway Analysis

Up-Stream Regulators (USR), Diseases and Functions and canonical pathways enriched in differentially expressed genes in direct and indirect interactions were investigated using Ingenuity Pathway Analysis (IPA) (QIAGEN).

Network Analysis

Protein interaction networks of differentially expressed gene lists were visualized in Cytoscape (v3.7.2) (Shannon et al., 2003). Enrichment for biological processes, molecular functions, KEGG pathways and other gene ontology categories in DEG lists was elucidated using the STRING database (Szklarczyk et al., 2019) and GO enrichment analysis (Mi et al., 2019).

Gene Set Enrichment Analysis

Preranked GSEA (Subramanian et al., 2005) was performed on a desktop application (GSEA v4.0.3) (http://www.broadinstitute.org/gsea/) using the "GSEAPreranked" module. Gene sets from the supplemental materials from the Winkler et al. (Winkler et al., 2020), Blanco-Melo et al. (Blanco-Melo et al., 2020) and Wu et al. (Wu et al., 2020b) (filename.GMT) studies were investigated for enrichment in our pre-ranked all gene list for SARS-CoV-2 infected day 2 mice lung comparing plus versus minus ACE2 (Supplementary Table 2B). Li et al. (Li et al., 2014) blood transcription modules (BTM_for_GSEA_20131008.gmt, n = 346) was also used in GSEA to determine enrichment in our 'immunized' versus unvaccinated mice lung at day 2 (Supplementary Table 5B). The complete Molecular Signatures Database (MSigDB) v7.2 gene set collection (31,120 gene sets) (msigdb.v7.2.symbols.gmt: https://www.gsea-msigdb.org/gsea/msigdb/download_file.jsp?filePath=/msigdb/release/7.2/msigdb.v7.2.symbols.gmt) was used to run GSEAs on pre-ranked gene list for plus versus minus ACE2 at day 2 (Supplementary Table 1B), and day 6 versus day 2 (Supplementary Table 2B). Gene ontology (Ashburner et al., 2000; Consortium, 2021) and Enrichr (Chen et al., 2013; Kuleshov et al., 2016) web-tools were also consulted.

Interferome

The indicated DEG lists were entered into Interferome (www.interferome.org) (Rusinova et al., 2013) with the following parameters: *In Vivo*, Mus musculus, fold change 2 (up and down).

Statistics

Statistical analyses of experimental data were performed using IBM SPSS Statistics for Windows, Version 19.0 (IBM Corp., Armonk, NY, USA). The t-test was used when the difference in variances was <4, skewness was >2 and kurtosis was <2. Otherwise, the non-parametric Kolmogorov–Smirnov test or Kruskal-Wallis test was used. Repeated Measures Two-Way ANOVA was used where indicated.

SUPPPLEMENTAL INFORMATION

Supplementary Figure 1. Replication of SARS-CoV-2 in hACE2-lentivirus transduced mouse cell lines. Growth kinetics of SARS-CoV-2 over a three day time course in untransduced or hACE2-lentivirus transduced 3T3 or AE17 cells infected at MOI=0.1. Data is the mean of triplicate wells and error bars represent SEM. Images of cells were taken using an inverted light microscope at day 3 post-infection and are representative of triplicate wells.

Supplementary Figure 2. RT-qPCR of mice lung RNA using primers for SARS-CoV-2 normalized to hACE2 introduced by lentivirus transduction. Data is individual mice from Figure 2E normalised to 2C, and is expressed as RNA copy number calculated against a standard curve for each gene.

Supplementary Figure 3. SARS-CoV-2 and hACE2 read counts in RNA-Seq data. RNA-Seq was performed on mice lung from the same mice as in 'Figure 2'. **A)** SARS-CoV-2 read counts normalized to total read count. Data points below the horizontal dotted line had read counts of zero. **B)** hACE2 read counts normalised to total read count. Data points below the horizontal dotted line had read counts of zero. **C)** SARS-CoV-2 read count normalised to hACE2 read count. Circle with pink dotted outline had hACE2 read count of 0, so the value was set to the SARS-CoV-2 read count (not normalised). **D)** SARS-CoV-2 reads aligned to reference genome viewed in Integrative Genome Viewer (IGV). Mice with hACE2 displayed reads mapped across the entire genome, with higher counts for structural gene sub-genomic RNA as also evident in hACE2-adenoviral vector transduced cell lines (Blanco-Melo et al., 2020).

Supplementary Table 1. RNA-Seq gene lists and downstream bioinformatic analyses of responses at day 2 post-infection.

Supplementary Table 2. RNA-Seq gene lists and downstream bioinformatic analyses of responses at day 6 post-infection.

Supplementary Table 3. RNA-Seq gene lists and downstream bioinformatic analyses of responses in IFNAR$^{-/-}$ versus C57BL/6J mice at day 2 post-infection.

Supplementary Table 4. RNA-Seq gene lists and downstream bioinformatic analyses of responses in IL-28RA$^{-/-}$ versus C57BL/6J mice at day 2 post-infection.

Supplementary Table 5. RNA-Seq gene lists and downstream bioinformatic analyses of responses in immunized versus unvaccinated mice at day 2 post-infection.

REFERENCES

Alexander, M.R., Schoeder, C.T., Brown, J.A., Smart, C.D., Moth, C., Wikswo, J.P., Capra, J.A., Meiler, J., Chen, W., and Madhur, M.S. (2020). Predicting susceptibility to SARS-CoV-2 infection based on structural differences in ACE2 across species. The FASEB Journal *34*, 15946-15960.

Alton, E.W., Beekman, J.M., Boyd, A.C., Brand, J., Carlon, M.S., Connolly, M.M., Chan, M., Conlon, S., Davidson, H.E., Davies, J.C., *et al.* (2017a). Preparation for a first-in-man lentivirus trial in patients with cystic fibrosis. Thorax *72*, 137-147.

Alton, E.W.F.W., Beekman, J.M., Boyd, A.C., Brand, J., Carlon, M.S., Connolly, M.M., Chan, M., Conlon, S., Davidson, H.E., Davies, J.C., *et al.* (2017b). Preparation for a first-in-man lentivirus trial in patients with cystic fibrosis. Thorax *72*, 137.

Ank, N., Iversen, M.B., Bartholdy, C., Staeheli, P., Hartmann, R., Jensen, U.B., Dagnaes-Hansen, F., Thomsen, A.R., Chen, Z., Haugen, H., *et al.* (2008). An Important Role for Type III Interferon (IFN-λ/IL-28) in TLR-Induced Antiviral Activity. The Journal of Immunology *180*, 2474-2485.

Ashburner, M., Ball, C.A., Blake, J.A., Botstein, D., Butler, H., Cherry, J.M., Davis, A.P., Dolinski, K., Dwight, S.S., Eppig, J.T., *et al.* (2000). Gene ontology: tool for the unification of biology. The Gene Ontology Consortium. Nature genetics *25*, 25-29.

Badawy, A.A.B. (2020). Immunotherapy of COVID-19 with poly (ADP-ribose) polymerase inhibitors: starting with nicotinamide. Biosci Rep *40*, BSR20202856.

843 Banerjee, A.K., Blanco, M.R., Bruce, E.A., Honson, D.D., Chen, L.M., Chow, A., Bhat, P., Ollikainen, N.,
844 Quinodoz, S.A., Loney, C., *et al.* (2020). SARS-CoV-2 Disrupts Splicing, Translation, and Protein Trafficking
845 to Suppress Host Defenses. Cell *183*, 1325-1339.e1321.
846 Bao, L., Deng, W., Huang, B., Gao, H., Liu, J., Ren, L., Wei, Q., Yu, P., Xu, Y., Qi, F., *et al.* (2020). The
847 pathogenicity of SARS-CoV-2 in hACE2 transgenic mice. Nature *583*, 830-833.
848 Blanco-Melo, D., Nilsson-Payant, B.E., Liu, W.C., Uhl, S., Hoagland, D., Møller, R., Jordan, T.X., Oishi, K.,
849 Panis, M., Sachs, D., *et al.* (2020). Imbalanced Host Response to SARS-CoV-2 Drives Development of
850 COVID-19. Cell *181*, 1036-1045.e1039.
851 Boudewijns, R., Thibaut, H.J., Kaptein, S.J.F., Li, R., Vergote, V., Seldeslachts, L., Van Weyenbergh, J., De
852 Keyzer, C., Bervoets, L., Sharma, S., *et al.* (2020). STAT2 signaling restricts viral dissemination but drives
853 severe pneumonia in SARS-CoV-2 infected hamsters. Nature Communications *11*, 5838.
854 Buckley, S.M.K., Howe, S.J., Sheard, V., Ward, N.J., Coutelle, C., Thrasher, A.J., Waddington, S.N., and
855 McKay, T.R. (2008). Lentiviral transduction of the murine lung provides efficient pseudotype and
856 developmental stage-dependent cell-specific transgene expression. Gene Therapy *15*, 1167-1175.
857 Carossino, M., Montanaro, P., O'Connell, A., Kenney, D., Gertje, H., Grosz, K.A., Kurnick, S.A., Bosmann,
858 M., Saeed, M., Balasuriya, U.B.R., *et al.* (2021). Fatal neuroinvasion of SARS-CoV-2 in K18-hACE2 mice is
859 partially dependent on hACE2 expression. bioRxiv.
860 Chan, K.K., Dorosky, D., Sharma, P., Abbasi, S.A., Dye, J.M., Kranz, D.M., Herbert, A.S., and Procko, E.
861 (2020). Engineering human ACE2 to optimize binding to the spike protein of SARS coronavirus 2. Science
862 (New York, NY) *369*, 1261-1265.
863 Channappanavar, R., Fehr, Anthony R., Vijay, R., Mack, M., Zhao, J., Meyerholz, David K., and Perlman, S.
864 (2016). Dysregulated Type I Interferon and Inflammatory Monocyte-Macrophage Responses Cause
865 Lethal Pneumonia in SARS-CoV-Infected Mice. Cell host & microbe *19*, 181-193.
866 Channappanavar, R., Fett, C., Mack, M., Ten Eyck, P.P., Meyerholz, D.K., and Perlman, S. (2017). Sex-
867 Based Differences in Susceptibility to Severe Acute Respiratory Syndrome Coronavirus Infection. J
868 Immunol *198*, 4046-4053.
869 Chen, E.Y., Tan, C.M., Kou, Y., Duan, Q., Wang, Z., Meirelles, G.V., Clark, N.R., and Ma'ayan, A. (2013).
870 Enrichr: interactive and collaborative HTML5 gene list enrichment analysis tool. BMC Bioinformatics *14*,
871 128.
872 Chlibek, R., Bayas, J.M., Collins, H., de la Pinta, M.L.R., Ledent, E., Mols, J.F., and Heineman, T.C. (2013).
873 Safety and Immunogenicity of an AS01-adjuvanted Varicella-zoster Virus Subunit Candidate Vaccine
874 Against Herpes Zoster in Adults ≥50 Years of Age. The Journal of Infectious Diseases *208*, 1953-1961.
875 Consortium, G.O. (2021). The Gene Ontology resource: enriching a GOld mine. Nucleic Acids Res *49*,
876 D325-d334.
877 Copreni, E., Palmieri, L., Castellani, S., and Conese, M. (2010). A VSV-G Pseudotyped Last Generation
878 Lentiviral Vector Mediates High Level and Persistent Gene Transfer in Models of Airway Epithelium In
879 Vitro and In Vivo. Viruses *2*, 1577-1588.
880 Copreni, E., Penzo, M., Carrabino, S., and Conese, M. (2004). Lentivirus-mediated gene transfer to the
881 respiratory epithelium: a promising approach to gene therapy of cystic fibrosis. Gene Therapy *11*, S67-
882 S75.
883 Crawford, K.H.D., Eguia, R., Dingens, A.S., Loes, A.N., Malone, K.D., Wolf, C.R., Chu, H.Y., Tortorici, M.A.,
884 Veesler, D., Murphy, M., *et al.* (2020). Protocol and Reagents for Pseudotyping Lentiviral Particles with
885 SARS-CoV-2 Spike Protein for Neutralization Assays. Viruses *12*.
886 Curtin, N., Bányai, K., Thaventhiran, J., Le Quesne, J., Helyes, Z., and Bai, P. (2020). Repositioning PARP
887 inhibitors for SARS-CoV-2 infection(COVID-19); a new multi-pronged therapy for acute respiratory
888 distress syndrome? British Journal of Pharmacology *177*, 3635-3645.
889 Damas, J., Hughes, G.M., Keough, K.C., Painter, C.A., Persky, N.S., Corbo, M., Hiller, M., Koepfli, K.-P.,
890 Pfenning, A.R., Zhao, H., *et al.* (2020). Broad host range of SARS-CoV-2 predicted by comparative and

891 structural analysis of ACE2 in vertebrates. Proceedings of the National Academy of Sciences *117*, 22311-
892 22322.
893 Dinnon, K.H., Leist, S.R., Schäfer, A., Edwards, C.E., Martinez, D.R., Montgomery, S.A., West, A., Yount,
894 B.L., Hou, Y.J., Adams, L.E.*, et al.* (2020). A mouse-adapted model of SARS-CoV-2 to test COVID-19
895 countermeasures. Nature *586*, 560-566.
896 Dobin, A., Davis, C.A., Schlesinger, F., Drenkow, J., Zaleski, C., Jha, S., Batut, P., Chaisson, M., and
897 Gingeras, T.R. (2013). STAR: ultrafast universal RNA-seq aligner. Bioinformatics *29*, 15-21.
898 Duperray, C., Boiron, J.M., Boucheix, C., Cantaloube, J.F., Lavabre-Bertrand, T., Attal, M., Brochier, J.,
899 Maraninchi, D., Bataille, R., and Klein, B. (1990). The CD24 antigen discriminates between pre-B and B
900 cells in human bone marrow. J Immunol *145*, 3678-3683.
901 Felgenhauer, U., Schoen, A., Gad, H.H., Hartmann, R., Schaubmar, A.R., Failing, K., Drosten, C., and
902 Weber, F. (2020). Inhibition of SARS-CoV-2 by type I and type III interferons. J Biol Chem *295*, 13958-
903 13964.
904 Frieman, M.B., Chen, J., Morrison, T.E., Whitmore, A., Funkhouser, W., Ward, J.M., Lamirande, E.W.,
905 Roberts, A., Heise, M., Subbarao, K.*, et al.* (2010). SARS-CoV Pathogenesis Is Regulated by a STAT1
906 Dependent but a Type I, II and III Interferon Receptor Independent Mechanism. PLOS Pathogens *6*,
907 e1000849.
908 Gadotti, A.C., de Castro Deus, M., Telles, J.P., Wind, R., Goes, M., Garcia Charello Ossoski, R., de Padua,
909 A.M., de Noronha, L., Moreno-Amaral, A., Baena, C.P.*, et al.* (2020). IFN-γ is an independent risk factor
910 associated with mortality in patients with moderate and severe COVID-19 infection. Virus Res *289*,
911 198171-198171.
912 Galani, I.E., Triantafyllia, V., Eleminiadou, E.E., Koltsida, O., Stavropoulos, A., Manioudaki, M., Thanos, D.,
913 Doyle, S.E., Kotenko, S.V., Thanopoulou, K.*, et al.* (2017). Interferon-λ Mediates Non-redundant Front-
914 Line Antiviral Protection against Influenza Virus Infection without Compromising Host Fitness. Immunity
915 *46*, 875-890.e876.
916 Golden, J.W., Cline, C.R., Zeng, X., Garrison, A.R., Carey, B.D., Mucker, E.M., White, L.E., Shamblin, J.D.,
917 Brocato, R.L., Liu, J.*, et al.* (2020). Human angiotensin-converting enzyme 2 transgenic mice infected with
918 SARS-CoV-2 develop severe and fatal respiratory disease. JCI insight.
919 Griffin, B.D., Chan, M., Tailor, N., Mendoza, E.J., Leung, A., Warner, B.M., Duggan, A.T., Moffat, E., He, S.,
920 Garnett, L.*, et al.* (2020). North American deer mice are susceptible to SARS-CoV-2. bioRxiv,
921 2020.2007.2025.221291.
922 Gu, H., Chen, Q., Yang, G., He, L., Fan, H., Deng, Y.-Q., Wang, Y., Teng, Y., Zhao, Z., Cui, Y.*, et al.* (2020).
923 Adaptation of SARS-CoV-2 in BALB/c mice for testing vaccine efficacy. Science (New York, NY) *369*, 1603-
924 1607.
925 Guan, W.-j., Ni, Z.-y., Hu, Y., Liang, W.-h., Ou, C.-q., He, J.-x., Liu, L., Shan, H., Lei, C.-l., Hui, D.S.C.*, et al.*
926 (2020). Clinical Characteristics of Coronavirus Disease 2019 in China. New England Journal of Medicine
927 *382*, 1708-1720.
928 Hall, J.C., and Rosen, A. (2010). Type I interferons: crucial participants in disease amplification in
929 autoimmunity. Nat Rev Rheumatol *6*, 40-49.
930 Han, H., Ma, Q., Li, C., Liu, R., Zhao, L., Wang, W., Zhang, P., Liu, X., Gao, G., Liu, F.*, et al.* (2020). Profiling
931 serum cytokines in COVID-19 patients reveals IL-6 and IL-10 are disease severity predictors. Emerging
932 microbes & infections *9*, 1123-1130.
933 Harrow, J., Frankish, A., Gonzalez, J.M., Tapanari, E., Diekhans, M., Kokocinski, F., Aken, B.L., Barrell, D.,
934 Zadissa, A., Searle, S.*, et al.* (2012). GENCODE: the reference human genome annotation for The ENCODE
935 Project. Genome Res *22*, 1760-1774.
936 Hassan, A.O., Case, J.B., Winkler, E.S., Thackray, L.B., Kafai, N.M., Bailey, A.L., McCune, B.T., Fox, J.M.,
937 Chen, R.E., Alsoussi, W.B.*, et al.* (2020). A SARS-CoV-2 Infection Model in Mice Demonstrates Protection
938 by Neutralizing Antibodies. Cell *182*, 744-753.e744.

939 Herold, T., Jurinovic, V., Arnreich, C., Lipworth, B.J., Hellmuth, J.C., von Bergwelt-Baildon, M., Klein, M.,
940 and Weinberger, T. (2020). Elevated levels of IL-6 and CRP predict the need for mechanical ventilation in
941 COVID-19. Journal of Allergy and Clinical Immunology *146*, 128-136.e124.
942 Huang, C., Wang, Y., Li, X., Ren, L., Zhao, J., Hu, Y., Zhang, L., Fan, G., Xu, J., Gu, X.*, et al.* (2020). Clinical
943 features of patients infected with 2019 novel coronavirus in Wuhan, China. Lancet (London, England)
944 *395*, 497-506.
945 Israelow, B., Song, E., Mao, T., Lu, P., Meir, A., Liu, F., Alfajaro, M.M., Wei, J., Dong, H., Homer, R.J.*, et al.*
946 (2020). Mouse model of SARS-CoV-2 reveals inflammatory role of type I interferon signaling. The Journal
947 of experimental medicine *217*.
948 Jefferson, T., Spencer, E., Brassey, J., and Heneghan, C. (2020). Viral cultures for COVID-19 infectivity
949 assessment. Systematic review. medRxiv, 2020.2008.2004.20167932.
950 Jiang, H.-w., Zhang, H.-n., Meng, Q.-f., Xie, J., Li, Y., Chen, H., Zheng, Y.-x., Wang, X.-n., Qi, H., Zhang, J.*, et*
951 *al.* (2020a). SARS-CoV-2 Orf9b suppresses type I interferon responses by targeting TOM70. Cellular &
952 Molecular Immunology *17*, 998-1000.
953 Jiang, R.-D., Liu, M.-Q., Chen, Y., Shan, C., Zhou, Y.-W., Shen, X.-R., Li, Q., Zhang, L., Zhu, Y., Si, H.-R.*, et al.*
954 (2020b). Pathogenesis of SARS-CoV-2 in Transgenic Mice Expressing Human Angiotensin-Converting
955 Enzyme 2. Cell *182*, 50-58.e58.
956 Jin, J.-M., Bai, P., He, W., Wu, F., Liu, X.-F., Han, D.-M., Liu, S., and Yang, J.-K. (2020). Gender Differences
957 in Patients With COVID-19: Focus on Severity and Mortality. Frontiers in Public Health *8*.
958 Johnson, B.J., Le, T.T., Dobbin, C.A., Banovic, T., Howard, C.B., Flores Fde, M., Vanags, D., Naylor, D.J.,
959 Hill, G.R., and Suhrbier, A. (2005). Heat shock protein 10 inhibits lipopolysaccharide-induced
960 inflammatory mediator production. J Biol Chem *280*, 4037-4047.
961 Kremer, K.L., Dunning, K.R., Parsons, D.W., and Anson, D.S. (2007). Gene delivery to airway epithelial
962 cells in vivo: a direct comparison of apical and basolateral transduction strategies using pseudotyped
963 lentivirus vectors. The journal of gene medicine *9*, 362-368.
964 Kuleshov, M.V., Jones, M.R., Rouillard, A.D., Fernandez, N.F., Duan, Q., Wang, Z., Koplev, S., Jenkins, S.L.,
965 Jagodnik, K.M., Lachmann, A.*, et al.* (2016). Enrichr: a comprehensive gene set enrichment analysis web
966 server 2016 update. Nucleic Acids Res *44*, W90-97.
967 Kumari, P., Rothan, H.A., Natekar, J.P., Stone, S., Pathak, H., Strate, P.G., Arora, K., Brinton, M.A., and
968 Kumar, M. (2020). Neuroinvasion and encephalitis following intranasal inoculation of SARS-CoV-2 in K18-
969 hACE2 mice. bioRxiv, 2020.2012.2014.422714.
970 La Linn, M., Bellett, A.J., Parsons, P.G., and Suhrbier, A. (1995). Complete removal of mycoplasma from
971 viral preparations using solvent extraction. J Virol Methods *52*, 51-54.
972 Lavoie, H., Gagnon, J., and Therrien, M. (2020). ERK signalling: a master regulator of cell behaviour, life
973 and fate. Nature Reviews Molecular Cell Biology *21*, 607-632.
974 Lazear, H.M., Schoggins, J.W., and Diamond, M.S. (2019). Shared and Distinct Functions of Type I and
975 Type III Interferons. Immunity *50*, 907-923.
976 Leist, S.R., Dinnon, K.H., 3rd, Schäfer, A., Tse, L.V., Okuda, K., Hou, Y.J., West, A., Edwards, C.E., Sanders,
977 W., Fritch, E.J.*, et al.* (2020). A Mouse-Adapted SARS-CoV-2 Induces Acute Lung Injury and Mortality in
978 Standard Laboratory Mice. Cell.
979 Li, B., and Dewey, C.N. (2011). RSEM: accurate transcript quantification from RNA-Seq data with or
980 without a reference genome. BMC Bioinformatics *12*, 323.
981 Li, H., Handsaker, B., Wysoker, A., Fennell, T., Ruan, J., Homer, N., Marth, G., Abecasis, G., and Durbin, R.
982 (2009). The Sequence Alignment/Map format and SAMtools. Bioinformatics *25*, 2078-2079.
983 Li, S., Rouphael, N., Duraisingham, S., Romero-Steiner, S., Presnell, S., Davis, C., Schmidt, D.S., Johnson,
984 S.E., Milton, A., Rajam, G.*, et al.* (2014). Molecular signatures of antibody responses derived from a
985 systems biology study of five human vaccines. Nature immunology *15*, 195-204.

986 Limberis, M., Anson, D.S., Fuller, M., and Parsons, D.W. (2002). Recovery of airway cystic fibrosis
987 transmembrane conductance regulator function in mice with cystic fibrosis after single-dose lentivirus-
988 mediated gene transfer. Human gene therapy *13*, 1961-1970.
989 Limberis, M.P., Bell, C.L., Heath, J., and Wilson, J.M. (2010). Activation of transgene-specific T cells
990 following lentivirus-mediated gene delivery to mouse lung. Mol Ther *18*, 143-150.
991 Lin, L., Han, Q., Xiong, Y., Li, T., Liu, Z., Xu, H., Wu, Y., Wang, N., and Liu, X. (2017). Krüpple-like-factor 4
992 Attenuates Lung Fibrosis via Inhibiting Epithelial-mesenchymal Transition. Scientific reports *7*, 15847-
993 15847.
994 Lu, L., Zhang, H., Dauphars, D.J., and He, Y.-W. (2021). A Potential Role of Interleukin 10 in COVID-19
995 Pathogenesis. Trends in Immunology *42*, 3-5.
996 Mahlakõiv, T., Ritz, D., Mordstein, M., DeDiego, M.L., Enjuanes, L., Müller, M.A., Drosten, C., and
997 Staeheli, P. (2012). Combined action of type I and type III interferon restricts initial replication of severe
998 acute respiratory syndrome coronavirus in the lung but fails to inhibit systemic virus spread. The Journal
999 of general virology *93*, 2601-2605.
1000 Martin, M. (2011). Cutadapt removes adapter sequences from high-throughput sequencing reads. 2011
1001 *17*, 3.
1002 Masiá, M., Fernández-González, M., Padilla, S., Ortega, P., García, J.A., Agulló, V., García-Abellán, J.,
1003 Telenti, G., Guillén, L., and Gutiérrez, F. (2020). Impact of interleukin-6 blockade with tocilizumab on
1004 SARS-CoV-2 viral kinetics and antibody responses in patients with COVID-19: A prospective cohort study.
1005 EBioMedicine *60*.
1006 McCray, P.B., Jr., Pewe, L., Wohlford-Lenane, C., Hickey, M., Manzel, L., Shi, L., Netland, J., Jia, H.P.,
1007 Halabi, C., Sigmund, C.D.*, et al.* (2007). Lethal infection of K18-hACE2 mice infected with severe acute
1008 respiratory syndrome coronavirus. Journal of virology *81*, 813-821.
1009 Mehdipour, A.R., and Hummer, G. (2020). Dual nature of human ACE2 glycosylation in binding to SARS-
1010 CoV-2 spike. bioRxiv, 2020.2007.2009.193680.
1011 Mi, H., Muruganujan, A., Ebert, D., Huang, X., and Thomas, P.D. (2019). PANTHER version 14: more
1012 genomes, a new PANTHER GO-slim and improvements in enrichment analysis tools. Nucleic Acids Res *47*,
1013 D419-d426.
1014 Miller, B., Silverstein, A., Flores, M., Cao, K., Kumagai, H., Mehta, H.H., Yen, K., Kim, S.-J., and Cohen, P.
1015 (2021). Host mitochondrial transcriptome response to SARS-CoV-2 in multiple cell models and clinical
1016 samples. Scientific Reports *11*, 3.
1017 Miorin, L., Kehrer, T., Sanchez-Aparicio, M.T., Zhang, K., Cohen, P., Patel, R.S., Cupic, A., Makio, T., Mei,
1018 M., Moreno, E.*, et al.* (2020). SARS-CoV-2 Orf6 hijacks Nup98 to block STAT nuclear import and
1019 antagonize interferon signaling. Proceedings of the National Academy of Sciences *117*, 28344.
1020 Monk, P.D., Marsden, R.J., Tear, V.J., Brookes, J., Batten, T.N., Mankowski, M., Gabbay, F.J., Davies, D.E.,
1021 Holgate, S.T., Ho, L.-P.*, et al.* (2020). Safety and efficacy of inhaled nebulised interferon beta-1a
1022 (SNG001) for treatment of SARS-CoV-2 infection: a randomised, double-blind, placebo-controlled, phase
1023 2 trial. The Lancet Respiratory Medicine.
1024 Moreau, G.B., Burgess, S.L., Sturek, J.M., Donlan, A.N., Petri, W.A., and Mann, B.J. (2020). Evaluation of
1025 K18-hACE2 Mice as a Model of SARS-CoV-2 Infection. The American journal of tropical medicine and
1026 hygiene *103*, 1215-1219.
1027 Muñoz-Fontela, C., Dowling, W.E., Funnell, S.G.P., Gsell, P.-S., Riveros-Balta, A.X., Albrecht, R.A.,
1028 Andersen, H., Baric, R.S., Carroll, M.W., Cavaleri, M.*, et al.* (2020). Animal models for COVID-19. Nature
1029 *586*, 509-515.
1030 Nechanitzky, R., Akbas, D., Scherer, S., Györy, I., Hoyler, T., Ramamoorthy, S., Diefenbach, A., and
1031 Grosschedl, R. (2013). Transcription factor EBF1 is essential for the maintenance of B cell identity and
1032 prevention of alternative fates in committed cells. Nature immunology *14*, 867-875.

1033 Nguyen, T.H., McAuley, J.L., Kim, Y., Zheng, M.Z., Gherardin, N.A., Godfrey, D.I., Purcell, D.F., Sullivan,
1034 L.C., Westall, G.P., Reading, P.C., *et al.* (2021). Influenza, but not SARS-CoV-2, infection induces a rapid
1035 interferon response that wanes with age and diminished tissue-resident memory CD8(+) T cells. Clin
1036 Transl Immunology *10*, e1242-e1242.
1037 Nicks, K.M., Fowler, T.W., Akel, N.S., Perrien, D.S., Suva, L.J., and Gaddy, D. (2010). Bone turnover across
1038 the menopause transition : The role of gonadal inhibins. Ann N Y Acad Sci *1192*, 153-160.
1039 Oladunni, F.S., Park, J.-G., Pino, P.A., Gonzalez, O., Akhter, A., Allué-Guardia, A., Olmo-Fontánez, A.,
1040 Gautam, S., Garcia-Vilanova, A., Ye, C., *et al.* (2020). Lethality of SARS-CoV-2 infection in K18 human
1041 angiotensin-converting enzyme 2 transgenic mice. Nature Communications *11*, 6122.
1042 Park, A., and Iwasaki, A. (2020). Type I and Type III Interferons - Induction, Signaling, Evasion, and
1043 Application to Combat COVID-19. Cell host & microbe *27*, 870-878.
1044 Peckham, H., de Gruijter, N.M., Raine, C., Radziszewska, A., Ciurtin, C., Wedderburn, L.R., Rosser, E.C.,
1045 Webb, K., and Deakin, C.T. (2020). Male sex identified by global COVID-19 meta-analysis as a risk factor
1046 for death and ITU admission. Nature Communications *11*, 6317.
1047 Pence, B.D. (2020). Severe COVID-19 and aging: are monocytes the key? Geroscience *42*, 1051-1061.
1048 Pinna, G. (2021). Sex and COVID-19: A Protective Role for Reproductive Steroids. Trends in
1049 endocrinology and metabolism: TEM *32*, 3-6.
1050 Raslan, A.A., and Yoon, J.K. (2020). WNT Signaling in Lung Repair and Regeneration. Mol Cells *43*, 774-
1051 783.
1052 Rathnasinghe, R., Strohmeier, S., Amanat, F., Gillespie, V.L., Krammer, F., García-Sastre, A., Coughlan, L.,
1053 Schotsaert, M., and Uccellini, M. (2020). Comparison of Transgenic and Adenovirus hACE2 Mouse
1054 Models for SARS-CoV-2 Infection. Emerging microbes & infections, 1-19.
1055 Rodrigues, J.P.G.L.M., Barrera-Vilarmau, S., M. C. Teixeira, J., Sorokina, M., Seckel, E., Kastritis, P.L., and
1056 Levitt, M. (2020). Insights on cross-species transmission of SARS-CoV-2 from structural modeling. PLOS
1057 Computational Biology *16*, e1008449.
1058 Rusinova, I., Forster, S., Yu, S., Kannan, A., Masse, M., Cumming, H., Chapman, R., and Hertzog, P.J.
1059 (2013). INTERFEROME v2.0: an updated database of annotated interferon-regulated genes. Nucleic Acids
1060 Research *41*, D1040-D1046.
1061 Schroder, W.A., Le, T.T.T., Major, L., Street, S., Gardner, J., Lambley, E., Markey, K., MacDonald, K.P.,
1062 Fish, R.J., Thomas, R., *et al.* (2010). A Physiological Function of Inflammation-Associated SerpinB2 Is
1063 Regulation of Adaptive Immunity. The Journal of Immunology *184*, 2663.
1064 Schubert, K., Karousis, E.D., Jomaa, A., Scaiola, A., Echeverria, B., Gurzeler, L.-A., Leibundgut, M., Thiel,
1065 V., Mühlemann, O., and Ban, N. (2020). SARS-CoV-2 Nsp1 binds the ribosomal mRNA channel to inhibit
1066 translation. Nature Structural & Molecular Biology *27*, 959-966.
1067 Shannon, P., Markiel, A., Ozier, O., Baliga, N.S., Wang, J.T., Ramage, D., Amin, N., Schwikowski, B., and
1068 Ideker, T. (2003). Cytoscape: a software environment for integrated models of biomolecular interaction
1069 networks. Genome Res *13*, 2498-2504.
1070 Simons, A. (2010). A quality control tool for high throughput sequence data. Available online:
1071 https://www.bioinformatics.babraham.ac.uk/projects/fastqc.
1072 Sountoulidis, A., Stavropoulos, A., Giaglis, S., Apostolou, E., Monteiro, R., Chuva de Sousa Lopes, S.M.,
1073 Chen, H., Stripp, B.R., Mummery, C., Andreakos, E., *et al.* (2012). Activation of the Canonical Bone
1074 Morphogenetic Protein (BMP) Pathway during Lung Morphogenesis and Adult Lung Tissue Repair. PLOS
1075 ONE *7*, e41460.
1076 Subramanian, A., Tamayo, P., Mootha, V.K., Mukherjee, S., Ebert, B.L., Gillette, M.A., Paulovich, A.,
1077 Pomeroy, S.L., Golub, T.R., Lander, E.S., *et al.* (2005). Gene set enrichment analysis: a knowledge-based
1078 approach for interpreting genome-wide expression profiles. Proc Natl Acad Sci U S A *102*, 15545-15550.

1079 Sun, J., Zhuang, Z., Zheng, J., Li, K., Wong, R.L.-Y., Liu, D., Huang, J., He, J., Zhu, A., Zhao, J., *et al.* (2020a).
1080 Generation of a Broadly Useful Model for COVID-19 Pathogenesis, Vaccination, and Treatment. Cell *182*,
1081 734-743.e735.
1082 Sun, S.H., Chen, Q., Gu, H.J., Yang, G., Wang, Y.X., Huang, X.Y., Liu, S.S., Zhang, N.N., Li, X.F., Xiong, R., *et*
1083 *al.* (2020b). A Mouse Model of SARS-CoV-2 Infection and Pathogenesis. Cell host & microbe *28*, 124-
1084 133.e124.
1085 Swann, J.B., Hayakawa, Y., Zerafa, N., Sheehan, K.C., Scott, B., Schreiber, R.D., Hertzog, P., and Smyth,
1086 M.J. (2007). Type I IFN contributes to NK cell homeostasis, activation, and antitumor function. J Immunol
1087 *178*, 7540-7549.
1088 Szklarczyk, D., Gable, A.L., Lyon, D., Junge, A., Wyder, S., Huerta-Cepas, J., Simonovic, M., Doncheva,
1089 N.T., Morris, J.H., Bork, P., *et al.* (2019). STRING v11: protein-protein association networks with increased
1090 coverage, supporting functional discovery in genome-wide experimental datasets. Nucleic Acids Res *47*,
1091 D607-D613.
1092 Takasuka, N., Fujii, H., Takahashi, Y., Kasai, M., Morikawa, S., Itamura, S., Ishii, K., Sakaguchi, M., Ohnishi,
1093 K., Ohshima, M., *et al.* (2004). A subcutaneously injected UV-inactivated SARS coronavirus vaccine elicits
1094 systemic humoral immunity in mice. International immunology *16*, 1423-1430.
1095 Tan, A.T., Linster, M., Tan, C.W., Le Bert, N., Chia, W.N., Kunasegaran, K., Zhuang, Y., Tham, C.Y.L., Chia,
1096 A., Smith, G.J.D., *et al.* (2021). Early induction of functional SARS-CoV-2-specific T cells associates with
1097 rapid viral clearance and mild disease in COVID-19 patients. Cell Reports *34*, 108728.
1098 Tseng, C.T., Huang, C., Newman, P., Wang, N., Narayanan, K., Watts, D.M., Makino, S., Packard, M.M.,
1099 Zaki, S.R., Chan, T.S., *et al.* (2007). Severe acute respiratory syndrome coronavirus infection of mice
1100 transgenic for the human Angiotensin-converting enzyme 2 virus receptor. Journal of virology *81*, 1162-
1101 1173.
1102 Vanderheiden, A., Ralfs, P., Chirkova, T., Upadhyay, A.A., Zimmerman, M.G., Bedoya, S., Aoued, H.,
1103 Tharp, G.M., Pellegrini, K.L., Manfredi, C., *et al.* (2020). Type I and Type III Interferons Restrict SARS-CoV-
1104 2 Infection of Human Airway Epithelial Cultures. Journal of virology *94*, e00985-00920.
1105 Vaz de Paula, C.B., de Azevedo, M.L.V., Nagashima, S., Martins, A.P.C., Malaquias, M.A.S., Miggiolaro,
1106 A.F.R.d.S., da Silva Motta Júnior, J., Avelino, G., do Carmo, L.A.P., Carstens, L.B., *et al.* (2020). IL-4/IL-13
1107 remodeling pathway of COVID-19 lung injury. Scientific Reports *10*, 18689.
1108 Wajnberg, A., Amanat, F., Firpo, A., Altman, D.R., Bailey, M.J., Mansour, M., McMahon, M., Meade, P.,
1109 Mendu, D.R., Muellers, K., *et al.* (2020). Robust neutralizing antibodies to SARS-CoV-2 infection persist
1110 for months. Science (New York, NY) *370*, 1227.
1111 Wang, H., Kadlecek, T.A., Au-Yeung, B.B., Goodfellow, H.E.S., Hsu, L.-Y., Freedman, T.S., and Weiss, A.
1112 (2010). ZAP-70: an essential kinase in T-cell signaling. Cold Spring Harb Perspect Biol *2*, a002279-
1113 a002279.
1114 Wang, Q., Zhang, Y., Wu, L., Niu, S., Song, C., Zhang, Z., Lu, G., Qiao, C., Hu, Y., Yuen, K.-Y., *et al.* (2020).
1115 Structural and Functional Basis of SARS-CoV-2 Entry by Using Human ACE2. Cell *181*, 894-904.e899.
1116 Weiskopf, D., Schmitz, K.S., Raadsen, M.P., Grifoni, A., Okba, N.M.A., Endeman, H., van den Akker, J.P.C.,
1117 Molenkamp, R., Koopmans, M.P.G., van Gorp, E.C.M., *et al.* (2020). Phenotype and kinetics of SARS-CoV-
1118 2–specific T cells in COVID-19 patients with acute respiratory distress syndrome. Science Immunology *5*,
1119 eabd2071.
1120 Wilson, J.M. (2004). Adeno-associated virus and lentivirus pseudotypes for lung-directed gene therapy.
1121 Proceedings of the American Thoracic Society *1*, 309-314.
1122 Winkler, E.S., Bailey, A.L., Kafai, N.M., Nair, S., McCune, B.T., Yu, J., Fox, J.M., Chen, R.E., Earnest, J.T.,
1123 Keeler, S.P., *et al.* (2020). SARS-CoV-2 infection of human ACE2-transgenic mice causes severe lung
1124 inflammation and impaired function. Nature immunology.
1125 Wu, F., Zhao, S., Yu, B., Chen, Y.-M., Wang, W., Song, Z.-G., Hu, Y., Tao, Z.-W., Tian, J.-H., Pei, Y.-Y., *et al.*
1126 (2020a). A new coronavirus associated with human respiratory disease in China. Nature *579*, 265-269.

1127 Wu, M., Chen, Y., Xia, H., Wang, C., Tan, C.Y., Cai, X., Liu, Y., Ji, F., Xiong, P., Liu, R.*, et al.* (2020b).
1128 Transcriptional and proteomic insights into the host response in fatal COVID-19 cases. Proceedings of
1129 the National Academy of Sciences *117*, 28336.
1130 Xia, H., Cao, Z., Xie, X., Zhang, X., Chen, J.Y.-C., Wang, H., Menachery, V.D., Rajsbaum, R., and Shi, P.-Y.
1131 (2020). Evasion of Type I Interferon by SARS-CoV-2. Cell Reports *33*, 108234.
1132 Yan, K., Vet, L.J., Tang, B., Hobson-Peters, J., Rawle, D.J., Le, T.T., Larcher, T., Hall, R.A., and Suhrbier, A.
1133 (2020). A Yellow Fever Virus 17D Infection and Disease Mouse Model Used to Evaluate a Chimeric
1134 Binjari-Yellow Fever Virus Vaccine. Vaccines *8*.
1135 Yinda, C.K., Port, J.R., Bushmaker, T., Offei Owusu, I., Purushotham, J.N., Avanzato, V.A., Fischer, R.J.,
1136 Schulz, J.E., Holbrook, M.G., Hebner, M.J.*, et al.* (2021). K18-hACE2 mice develop respiratory disease
1137 resembling severe COVID-19. PLoS Pathog *17*, e1009195.
1138 Zhao, X., Chen, D., Szabla, R., Zheng, M., Li, G., Du, P., Zheng, S., Li, X., Song, C., Li, R.*, et al.* (2020). Broad
1139 and Differential Animal Angiotensin-Converting Enzyme 2 Receptor Usage by SARS-CoV-2. Journal of
1140 virology *94*.
1141 Zhou, P., Yang, X.-L., Wang, X.-G., Hu, B., Zhang, L., Zhang, W., Si, H.-R., Zhu, Y., Li, B., Huang, C.-L.*, et al.*
1142 (2020). A pneumonia outbreak associated with a new coronavirus of probable bat origin. Nature *579*,
1143 270-273.
1144 Zhu, Y., Wang, W., and Wang, X. (2015). Roles of transcriptional factor 7 in production of inflammatory
1145 factors for lung diseases. J Transl Med *13*, 273-273.

1146

Figure 1

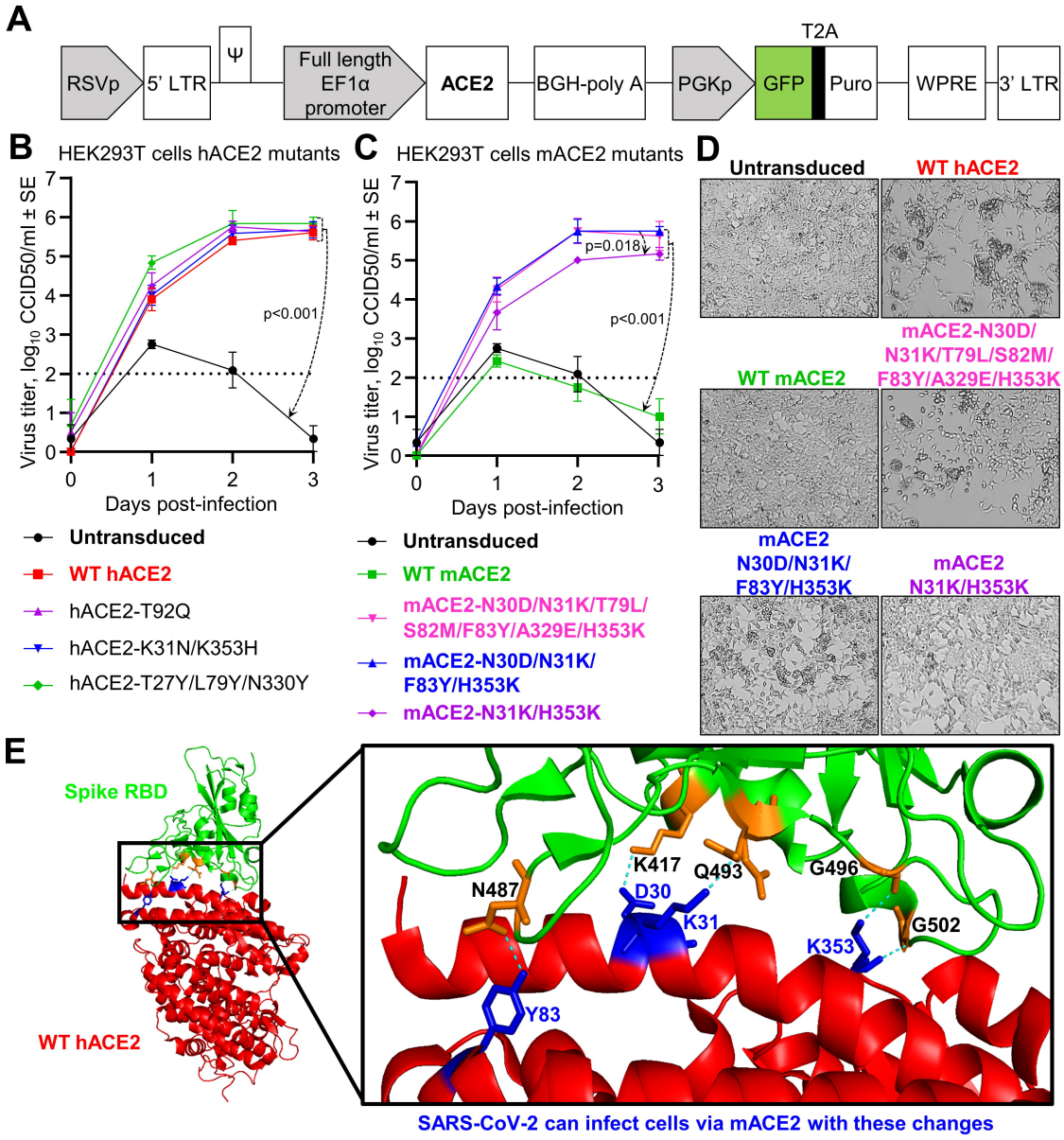
A
RSVp
5' LTR
Ψ
Full length EF1α promoter
ACE2
BGH-poly A
PGKp
T2A
GFP
Puro
WPRE
3' LTR
B
HEK293T cells hACE2 mutants
Virus titer, log10 CCID50/ml ± SE
Days post-infection
p<0.001
Untransduced
WT hACE2
hACE2-T92Q
hACE2-K31N/K353H
hACE2-T27Y/L79Y/N330Y
C
HEK293T cells mACE2 mutants
Virus titer, log10 CCID50/ml ± SE
Days post-infection
p=0.018
p<0.001
Untransduced
WT mACE2
mACE2-N30D/N31K/T79L/S82M/F83Y/A329E/H353K
mACE2-N30D/N31K/F83Y/H353K
mACE2-N31K/H353K
D
Untransduced
WT hACE2
WT mACE2
mACE2-N30D/N31K/T79L/S82M/F83Y/A329E/H353K
mACE2 N30D/N31K/F83Y/H353K
mACE2 N31K/H353K
E
Spike RBD
WT hACE2
N487
K417
D30
Q493
G496
K31
G502
K353
Y83
SARS-CoV-2 can infect cells via mACE2 with these changes

Figure 2

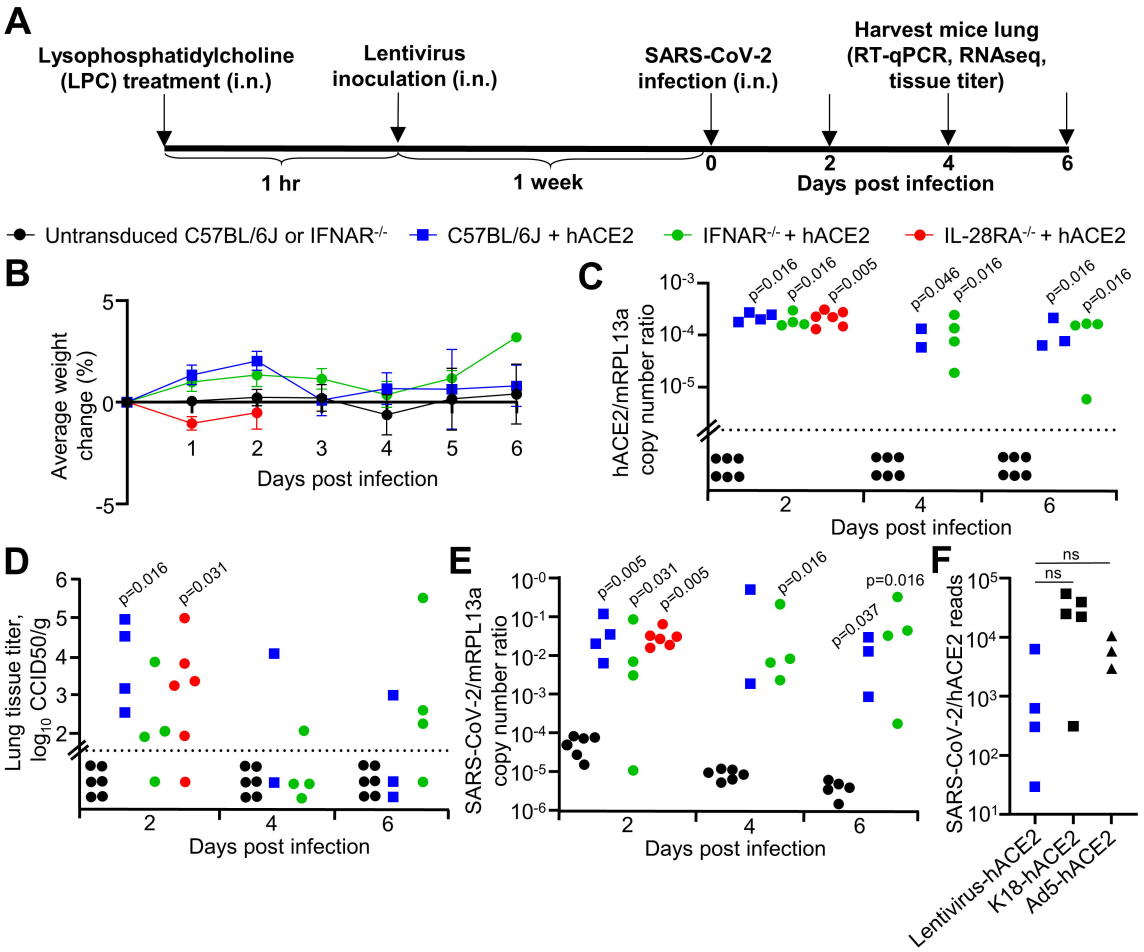
A
Lysophosphatidylcholine (LPC) treatment (i.n.)
Lentivirus inoculation (i.n.)
SARS-CoV-2 infection (i.n.)
Harvest mice lung (RT-qPCR, RNAseq, tissue titer)
1 hr
1 week
0
2
4
6
Days post infection
Untransduced C57BL/6J or IFNAR-/-
C57BL/6J + hACE2
IFNAR-/- + hACE2
IL-28RA-/- + hACE2
B
Average weight change (%)
Days post infection
C
hACE2/mRPL13a copy number ratio
p=0.016
p=0.016
p=0.005
p=0.046
p=0.016
p=0.016
p=0.016
Days post infection
D
Lung tissue titer, log10 CCID50/g
p=0.016
p=0.031
Days post infection
E
SARS-CoV-2/mRPL13a copy number ratio
p=0.005
p=0.031
p=0.005
p=0.016
p=0.037
p=0.016
Days post infection
F
SARS-CoV-2/hACE2 reads
ns
ns
Lentivirus-hACE2
K18-hACE2
Ad5-hACE2

Figure 3

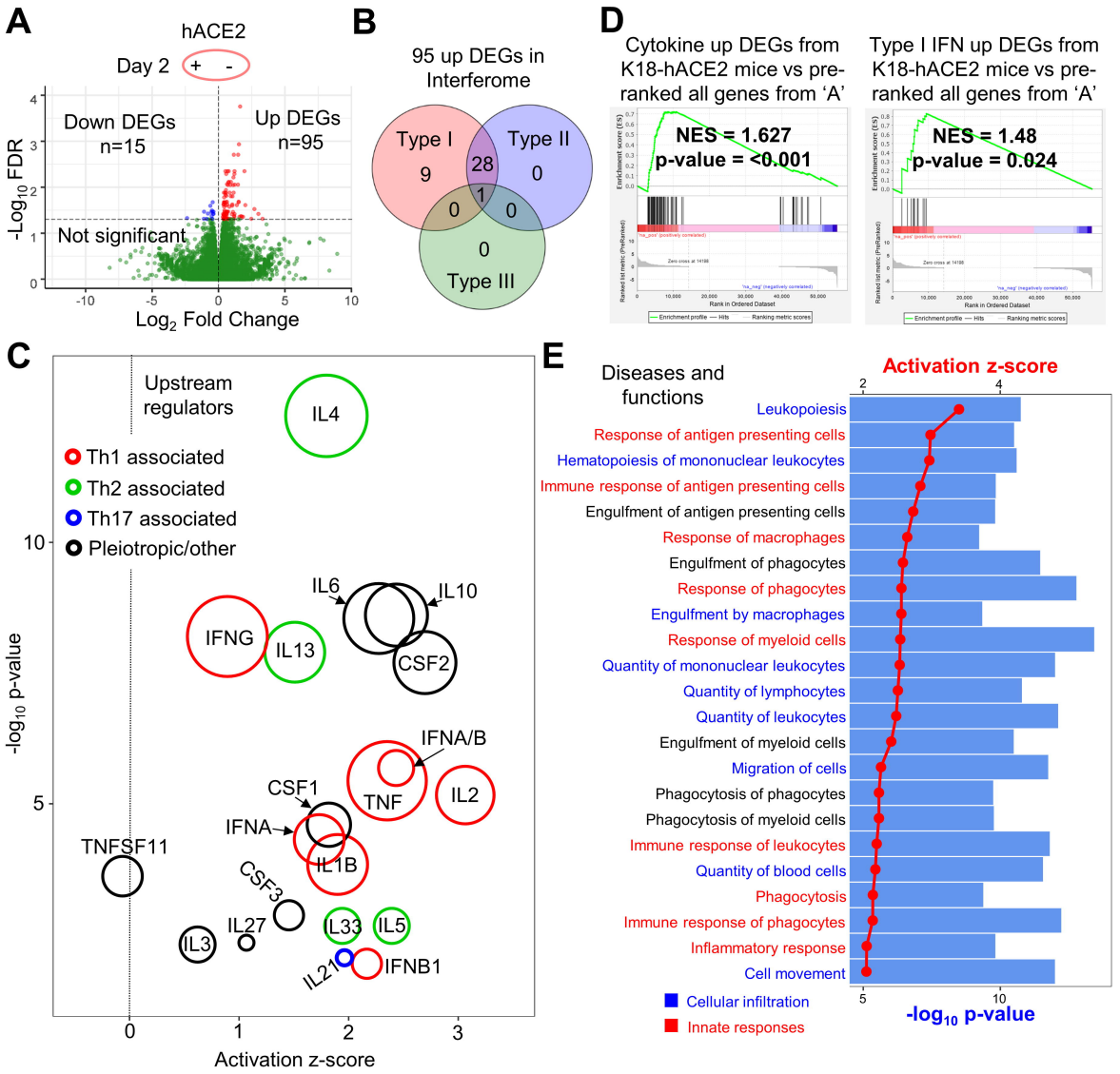

Core enriched genes analysed by GO Biological Processes ontology (Enrichr). Top 10 sorted by p-value:

GO process	P-value
cytokine-mediated signaling pathway	1.39E-20
cellular response to type I interferon	8.70E-20
type I interferon signaling pathway	8.70E-20
cellular response to interferon-gamma	4.33E-13
chemokine-mediated signaling pathway	6.10E-09
response to interferon-gamma	4.14E-08
inflammatory response	4.36E-08
lymphocyte chemotaxis	7.20E-08
eosinophil migration	1.01E-07
eosinophil chemotaxis	1.01E-07

Figure 4

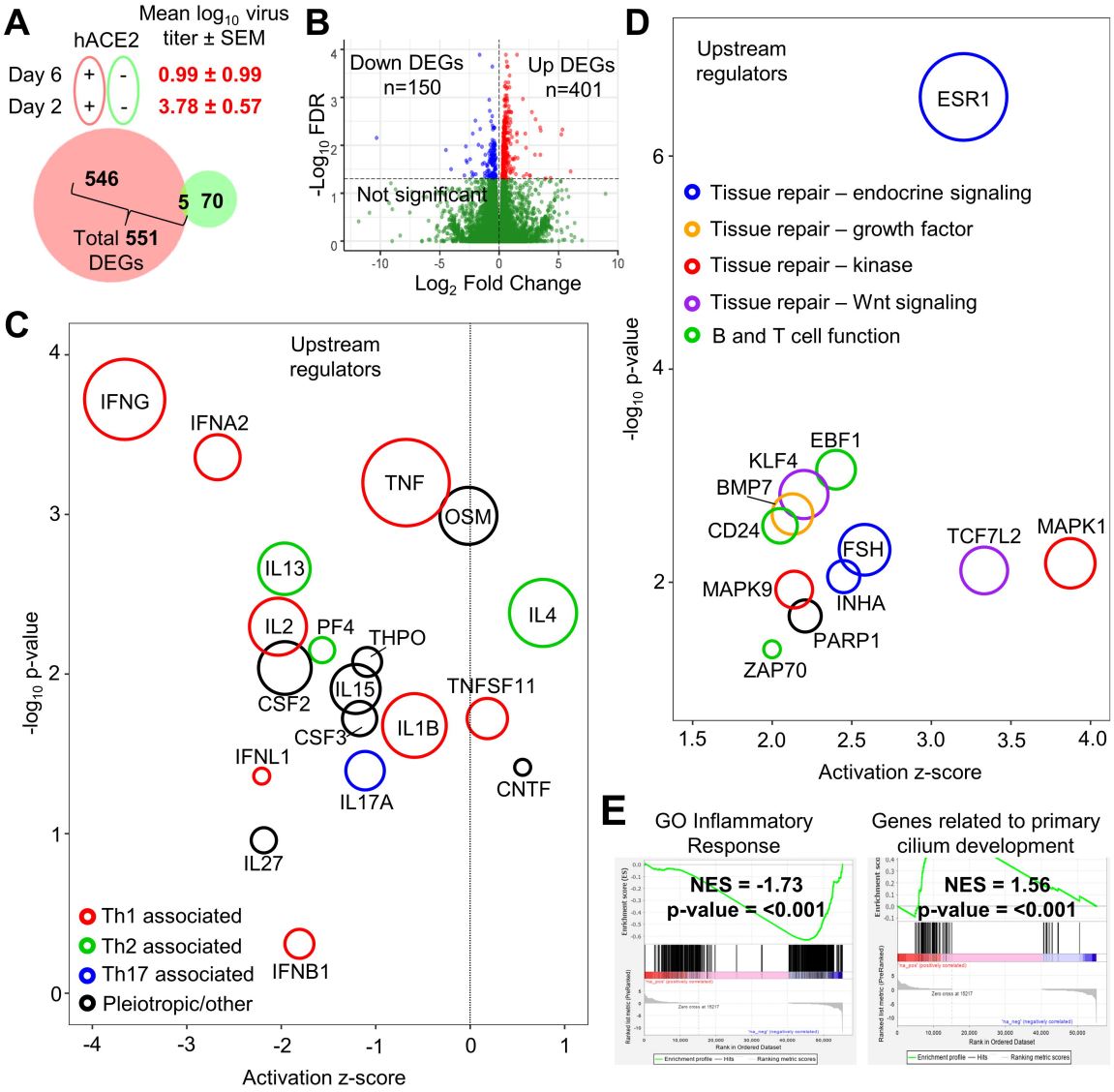
A
hACE2
Mean log10 virus titer ± SEM
Day 6 + - 0.99 ± 0.99
Day 2 + - 3.78 ± 0.57
546
5 70
Total 551 DEGs
B
Down DEGs n=150
Up DEGs n=401
Not significant
-Log10 FDR
Log2 Fold Change
C
Upstream regulators
IFNG
IFNA2
TNF
OSM
IL13
IL4
IL2
PF4
THPO
CSF2
IL15
TNFSF11
CSF3
IL1B
IFNL1
IL17A
CNTF
IL27
IFNB1
Th1 associated
Th2 associated
Th17 associated
Pleiotropic/other
-log10 p-value
Activation z-score
D
Upstream regulators
ESR1
Tissue repair – endocrine signaling
Tissue repair – growth factor
Tissue repair – kinase
Tissue repair – Wnt signaling
B and T cell function
EBF1
KLF4
BMP7
CD24
FSH
TCF7L2
MAPK1
MAPK9
INHA
PARP1
ZAP70
-log10 p-value
Activation z-score
E
GO Inflammatory Response
NES = -1.73
p-value = <0.001
Genes related to primary cilium development
NES = 1.56
p-value = <0.001

Figure 5

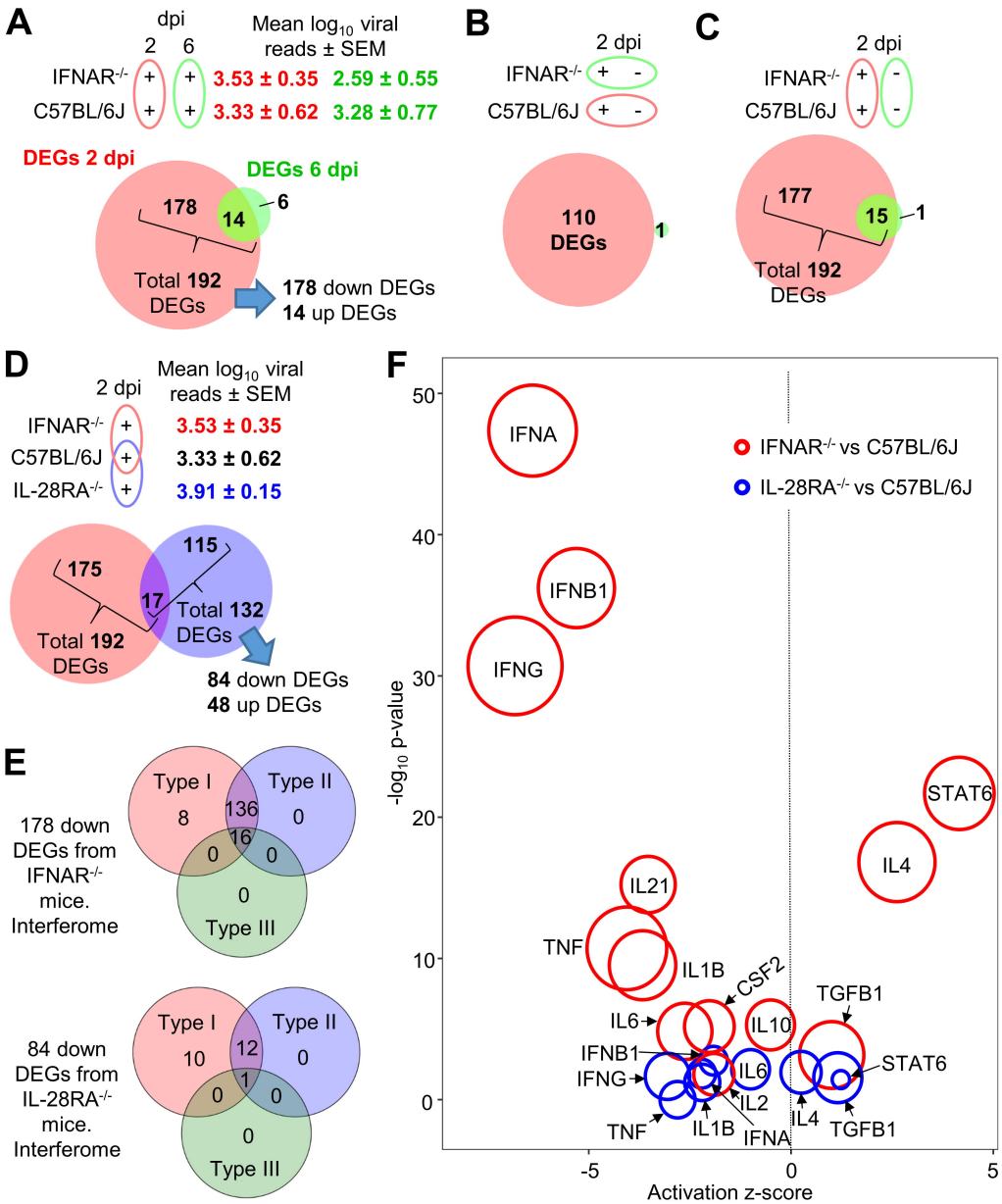
A
dpi
2 6
Mean log10 viral reads ± SEM
IFNAR-/- + + 3.53 ± 0.35 2.59 ± 0.55
C57BL/6J + + 3.33 ± 0.62 3.28 ± 0.77
DEGs 2 dpi
DEGs 6 dpi
178
14
6
Total 192 DEGs
178 down DEGs
14 up DEGs
B
2 dpi
IFNAR-/- + -
C57BL/6J + -
110 DEGs
1
C
2 dpi
IFNAR-/- + -
C57BL/6J + -
177
15
1
Total 192 DEGs
D
2 dpi
Mean log10 viral reads ± SEM
IFNAR-/- + 3.53 ± 0.35
C57BL/6J + 3.33 ± 0.62
IL-28RA-/- + 3.91 ± 0.15
175
115
17
Total 192 DEGs
Total 132 DEGs
84 down DEGs
48 up DEGs
E
178 down DEGs from IFNAR-/- mice. Interferome
Type I
Type II
Type III
8
136
0
16
0
0
0
84 down DEGs from IL-28RA-/- mice. Interferome
Type I
Type II
Type III
10
12
0
1
0
0
0
F
IFNAR-/- vs C57BL/6J
IL-28RA-/- vs C57BL/6J
-log10 p-value
Activation z-score
IFNA
IFNB1
IFNG
STAT6
IL4
IL21
TNF
IL1B
CSF2
TGFB1
IL6
IL10
IFNB1
IFNG
IL6
IL2
STAT6
TNF
IL1B
IFNA
IL4
TGFB1

Figure 6

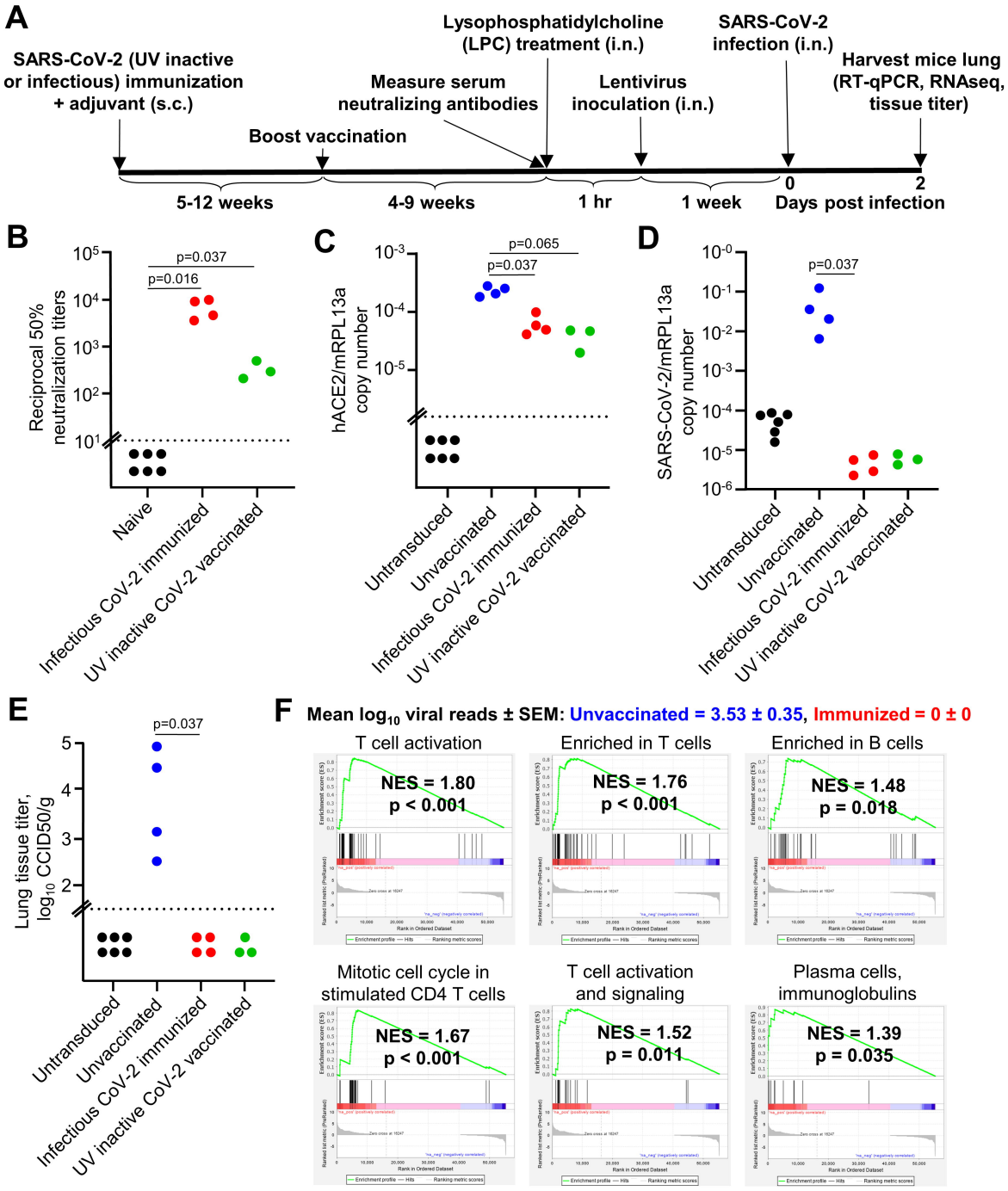
A
SARS-CoV-2 (UV inactive or infectious) immunization + adjuvant (s.c.)
Boost vaccination
Measure serum neutralizing antibodies
Lysophosphatidylcholine (LPC) treatment (i.n.)
Lentivirus inoculation (i.n.)
SARS-CoV-2 infection (i.n.)
Harvest mice lung (RT-qPCR, RNAseq, tissue titer)
5-12 weeks
4-9 weeks
1 hr
1 week
0
2
Days post infection
B
Reciprocal 50% neutralization titers
p=0.037
p=0.016
Naive
Infectious CoV-2 immunized
UV inactive CoV-2 vaccinated
C
hACE2/mRPL13a copy number
p=0.065
p=0.037
Untransduced
Unvaccinated
Infectious CoV-2 immunized
UV inactive CoV-2 vaccinated
D
SARS-CoV-2/mRPL13a copy number
p=0.037
Untransduced
Unvaccinated
Infectious CoV-2 immunized
UV inactive CoV-2 vaccinated
E
Lung tissue titer, log10 CCID50/g
p=0.037
Untransduced
Unvaccinated
Infectious CoV-2 immunized
UV inactive CoV-2 vaccinated
F
Mean log10 viral reads ± SEM: Unvaccinated = 3.53 ± 0.35, Immunized = 0 ± 0
T cell activation
NES = 1.80
p < 0.001
Enriched in T cells
NES = 1.76
p < 0.001
Enriched in B cells
NES = 1.48
p = 0.018
Mitotic cell cycle in stimulated CD4 T cells
NES = 1.67
p < 0.001
T cell activation and signaling
NES = 1.52
p = 0.011
Plasma cells, immunoglobulins
NES = 1.39
p = 0.035

Supplementary figure 1

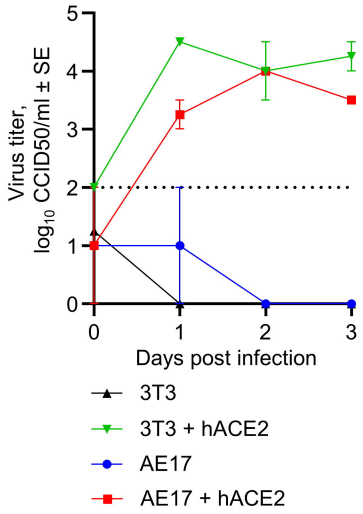

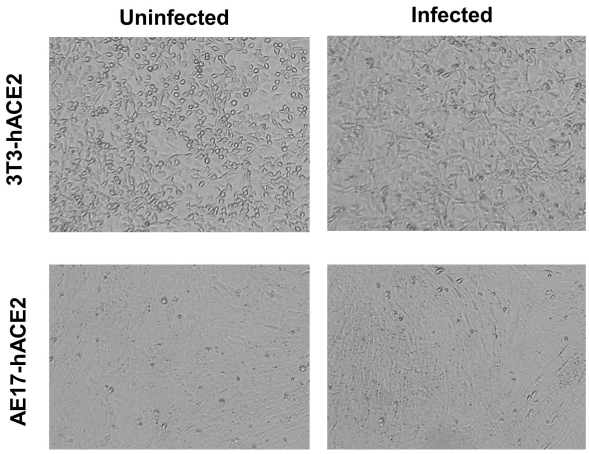

Supplementary figure 2

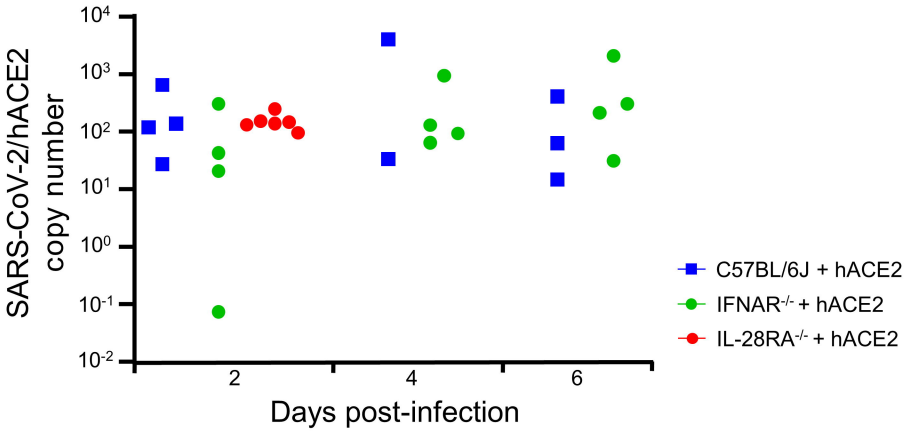
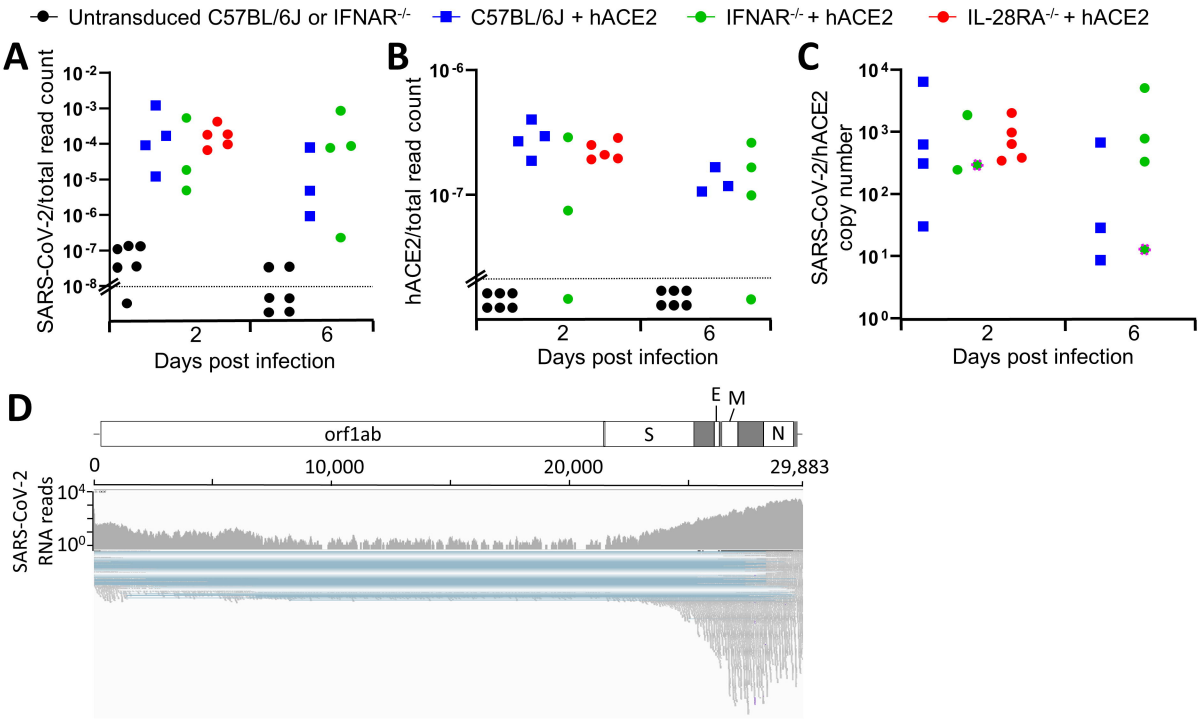
Supplementary figure 3